ISCI, Volume 7

Supplemental Information

Exploring Oxidation State-Dependent Selectivity in Polymerization of Cyclic Esters and Carbonates with Zinc(II) Complexes

Mark Abubekerov, Vojtěch Vlček, Junnian Wei, Matthias E. Miehlich, Stephanie M. Quan, Karsten Meyer, Daniel Neuhauser, and Paula L. Diaconescu

Table of Contents

Transparent Methods

General considerations. All reactions were performed using standard Schlenk techniques or in an MBraun drybox (<1 ppm O_2/H_2O), unless noted otherwise. All glassware, cannulas, and Celite were stored in an oven at > 425 K before being brought into the drybox. Solvents were purified using a two-column solid-state purification system by the method of Grubbs (Pangborn et al., 1996) and transferred to the glovebox without exposure to air. NMR solvents were obtained from Cambridge Isotope Laboratories, degassed, and stored over activated molecular sieves prior to use. NMR spectra were recorded at ambient temperature on Bruker AV-300, AV-400, AV-500, and DRX-500 spectrometers, unless otherwise noted. Proton and carbon chemical shifts are given relative to residual solvent peaks. Phosphorus, boron, and fluorine chemical shifts are given relative to external standards, H_3PO_4, $Et_2O{\cdot}BF_3$, and 1% Freon-113 in C_6D_6, respectively. Trimethoxybenzene was purchased from Sigma Aldrich and recrystallized from diethyl ether prior to use. L-lactide was purchased from TCI and recrystallized from THF prior to use. Liquid monomers were distilled over CaH_2 and brought into the box without exposure to air. Trimethylene carbonate (Matsuo et al., 1998), $[^{Ac}Fc][BAr^F]$ (Dhar et al., 2016), $(fc^{P,B})ZnCl{\cdot}(C_7H_8)$ (Abubekerov and Diaconescu, 2015), and $[(fc^{P,B})Zn(\mu\text{-}OCH_2Ph)]_2$ (Abubekerov et al., 2018) were prepared using literature procedures, and, unless otherwise noted, all reagents were acquired from commercial sources and used as received. Elemental analysis of $[(fc^{P,B})Zn(OCH_2Ph)]_2[BAr^F]_2$ was carried out by Midwest Microlab, LLC, Indianapolis, IN. Elemental analysis of $(fc^{P,B})Zn(OPh)$ was performed on an Exeter Analytical, Inc. CE-440 Elemental Analyzer. Molar masses of the polymers were determined by a MALS using a Shimazu Prominence-i LC 2030C 3D equipped with an autosampler, two MZ Analysentechnik MZ-Gel SDplus LS 5 μm, 300 × 8 mm linear columns, a Wyatt DAWN HELEOS-II, and a Wyatt Optilab T-rEX. The column temperature was

set at 40 °C. A flow rate of 0.70 mL/min was used, and samples were dissolved in chloroform. The number average molar mass and dispersity were found using the known concentration of the sample in chloroform with the assumption of 100% mass recovery to calculate d*n*/d*c* from the RI signal. Zero-field ^{57}Fe Mössbauer data were recorded on a WissEl spectrometer (MRG-500) at 77 K with alternating constant acceleration. ^{57}Co/Rh was used as the radiation source. The minimum experimental line width was 0.21 mm s^{-1} (full width at half-height). The temperature of the samples was controlled by an MBBC-HE0106 MÖSSBAUER He/N_2 cryostat within an accuracy of ±0.3 K. Isomer shifts were determined relative to α-iron at 298 K. Analysis and simulation of the data was done using the software "mcal" and "mf" written by E. Bill (Max Planck Institute for Chemical Energy Conversion, Mülheim an der Ruhr). All measurements were conducted with solid-state samples. The obtained solid was filled into PTFE (polytetrafluoroethylene) capsules in the glove box and placed in liquid nitrogen directly after being discharged from the glovebox. Handling and mounting of the samples were performed under liquid nitrogen. EPR spectra were recorded on a JEOL continuous wave spectrometer JES-FA200 equipped with an X-band Gunn oscillator bridge, a cylindrical mode cavity, and a helium cryostat. The samples were freshly dissolved in the respective solvent in an air-tight quartz EPR tube under nitrogen in the glovebox. The solution in the tube was frozen in liquid nitrogen upon exiting the glovebox and kept frozen until measured. Analysis and simulation of the data was done using the software "eview" and "esim" written by E. Bill (MPI for Chemical Energy Conversion, Mülheim an der Ruhr).

[(fc^{P,B})Zn(OCH$_2$Ph)]$_2$[BAr^F]$_2$. To solid [^{Ac}Fc][BAr^F] (67.8 mg, 0.062 mmol) was added [(fc^{P,B})Zn(μ-OCH$_2$Ph)]$_2$•(THF)$_2$ (55.8 mg, 0.034 mmol) in 4 mL of toluene/trifluorotoluene (1:1 vol %). The reaction mixture was stirred for 30 min at ambient temperature. The toluene solution

was decanted and the remaining oily red solids were washed with 2 × 2 mL of toluene. The product was isolated as a red solid after an hour under reduced pressure (77.8 mg, 78.0%). ^{1}H NMR (THF-d_8, 500 MHz, 298 K): δ (ppm) 2.24 (s), 2.39 (s), 4.40 (s), 4.43 (s), 4.63 (s), 4.66 (s), 6.07 (s), 7.09 (t), 7.14 (s), 7.28 (t), 7.58 (s), 7.71 (m), 7.79 (s), 8.95 (br s), 10.64 (br s). ^{11}B NMR (THF-d_8, 161 MHz, 298 K): δ (ppm) -5.9 (s), -7.8 (br s, $\Delta\nu_{1/2}$ = 289.2 Hz). ^{19}F NMR (THF-d_8, 376 MHz, 298 K): δ (ppm) -63.5 (s). Anal. Calcd: [($fc^{P,B}$)Zn(OCH_2Ph)][BAr^F] ($C_{71}H_{52}B_2F_{24}FeN_4OPZn$) C, 53.07; H, 3.26; N, 3.49. Found: C, 53.17; H, 3.32; N, 3.54.

($fc^{P,B}$)Zn(OPh). To ($fc^{P,B}$)ZnCl·(C_7H_8) (121.1 mg, 0.158 mmol) in 4 mL of methylene chloride was added solid NaOPh (27.6 mg, 0.238 mmol) and the suspension stirred for 1 h at ambient temperature. The reaction mixture was filtered through Celite and volatile substances were removed under reduced pressure. The remaining oily solids were dissolved in 2 mL of diethyl ether and stored at -35 °C for several hours. Decanting of the solution and washing with cold diethyl ether yielded the product as orange crystals (101.4 mg, 79.8%). X-ray quality crystals were obtained from diethyl ether at -35 °C. Crystals of ($fc^{P,B}$)Zn(OPh) always contain a molecule of diethyl ether per molecule of compound as supported by NMR data. ^{1}H NMR (C_6D_6, 500 MHz, 298 K): δ (ppm) 2.21 (s, 6H, C*H*$_3$), 2.27 (s, 6H, C*H*$_3$), 3.53 (q, 2H, Cp-*H*), 3.93(t, 2H, Cp-*H*), 4.00 (t, 2H, Cp-*H*), 4.04 (t, 2H, Cp-*H*), 4.70 (br s, 1H, B*H*), 5.69 (s, 2H, C*H*), 6.68 (m, 1H, *p*-Ph), 6.89 (m, 2H, *m*-Ph), 7.02 (m, 6H, *m*-Ph, *p*-Ph), 7.15 (m, 2H, *o*-Ph), 7.98 (m, 4H, *o*-Ph). ^{13}C NMR (C_6D_6, 126 MHz, 298 K): δ (ppm) 13.3 (s, *C*H$_3$), 14.0 (s, *C*H$_3$), 68.1 (d, Cp-*C*), 68.2 (s, Cp-*C*), 69.6 (s, Cp-*C*), 72.2 (d, Cp-*C*), 72.6 (s, Cp-*C*), 75.1 (s, Cp-*C*), 106.8 (s, *C*H), 115.4 (s, aromatic), 119.4 (s, aromatic), 129.3 (d, aromatic), 130.2 (s, aromatic), 131.2 (d, aromatic), 131.4 (d, aromatic), 134.5 (d, aromatic), 147.9 (s, *C*CH$_3$), 150.1 (s, *C*CH$_3$), 168.0 (d, aromatic). ^{31}P{^{1}H} NMR (C_6D_6, 203 MHz, 298 K): δ (ppm) -15.5 (s). ^{11}B NMR (C_6D_6, 161 MHz, 298 K): δ (ppm) -7.0 (br s, $\Delta\nu_{1/2}$ =

343.7 Hz). Anal. Calcd: ($fc^{P,B}$)Zn(OPh)·(Et_2O) ($C_{42}H_{48}BFeN_4O_2PZn$) C, 62.75; H, 6.02; N, 6.97. Found: C, 61.83; H, 5.81; N, 6.75.

NMR Scale Polymerizations. To a small vial, [($fc^{P,B}$)Zn(μ-OCH_2Ph)]$_2$ (2.5 μmol), an external standard, hexamethylbenzene (0.025 mmol), the monomer (0.5 mmol), and 0.5 mL of C_6D_6 were added. The contents of the vial were stirred and the homogeneous solution was transferred to a J. Young NMR tube equipped with a Teflon valve. The NMR tube was sealed, taken out of the box and placed in an oil bath. The polymerization was monitored by ^{1}H NMR spectroscopy until the conversion stopped or reached completion. The contents of the NMR tube were diluted with 0.5 mL of dichloromethane and poured into 10 mL of methanol to yield white solids. The product was collected on a glass frit, washed with additional 5 mL of methanol and kept under reduced pressure until it reached a consistent weight. For the control experiments, [^{Ac}Fc][BAr^F] (5 μmol) was used instead of [($fc^{P,B}$)Zn(μ-OCH_2Ph)]$_2$ under similar conditions as above (Figures S14-S17).

Electrochemical studies. Cyclic voltammetry studies were carried out in a 20 mL scintillation vial with electrodes fixed in position by a rubber stopper, in a 0.10 M tetrabutylammonium hexafluorophosphate solution in THF. A glassy carbon working electrode (planar circular area = 0.071 cm^2), a platinum reference electrode (planar circular area = 0.031 cm^2), and a silver-wire pseudo-reference electrode were purchased from CH Instruments. Before each cyclic voltammogram was recorded, the working and auxiliary electrodes were polished with an aqueous suspension of 0.05 μm alumina on a Microcloth polishing pad. Cyclic voltammograms were acquired with a CH Instruments CHI630D potentiostat and recorded with CH Instruments software (version 13.04) with data processing on Origin 9.2. All potentials are given with respect to the ferrocene-ferrocenium couple.

X-ray crystallography. X-ray quality crystals were obtained from various concentrated solutions placed in a -35 °C freezer in the glove box unless otherwise specified. Inside the glove box, the crystals were coated with oil (STP Oil Treatment) on a microscope slide, which was brought outside the glove box. The X-ray data collections were carried out on a Bruker SMART 1000 single crystal X-ray diffractometer using MoK_{α} radiation and a SMART APEX CCD detector. The data was reduced by SAINTPLUS and an empirical absorption correction was applied using the package SADABS. The structure was solved and refined using SHELXTL (Brucker 1998, SMART, SAINT, XPREP, AND SHELXTL, Brucker AXS Inc., Madison, Wiscosin, USA). Tables with atomic coordinates and equivalent isotropic displacement parameters, with all the distances and angles, and with anisotropic displacement parameters are listed in the cif.

DFT calculations. All calculations were carried out with the GAUSSIAN 09 program package. Geometry optimizations were performed with B3LYP (Becke, 1993a, Lee et al., 1988, Becke, 1993b). The LANL2DZ basis set (Hay and Wadt, 1985, Roy et al., 2008, Ehlers et al., 1993) with ECP was used for Zn and Fe, and the 6-31G(d) basis set (Ditchfield et al., 1971, Hehre et al., 1972, Hariharan and Pople, 1973) was used for other atoms. Frequency analysis was conducted at the same level of theory to verify that the stationary points are minima or saddle points. The single point energies and solvent effects in benzene were computed with PBE1PBE (Perdew et al., 1996) / SDD-6-311+G(d,p) basis sets (Dolg et al., 1987) by using the PCM solvation model (Scalmani and Frisch, 2010). The D3 version of Grimme's dispersion was applied for the dispersion correction (Grimme et al., 2010). All enthalpies and the Gibbs free energies are given in Hartree.

Electronic structure calculations. The electronic structure of the system was investigated with the Quantum Espresso software package (Paolo et al., 2009) by using the geometry optimized with

Gaussian 09 (see “DFT calculations” paragraph). For the exchange-correlation, a PBE generalized gradient approximation was used. This approach was combined with a U parameter obtained with the approach of Cococcioni & de Gironcoli (Cococcioni and de Gironcoli, 2005). Projected augmented wave pseudopotentials were used for all atoms. The kinetic energy cutoffs were 50 and 400 Ry for the planewave and density expansions, respectively. The total energy was converged to 0.05 Ry and the eigenvalues to 0.01 eV.

NMR Spectra

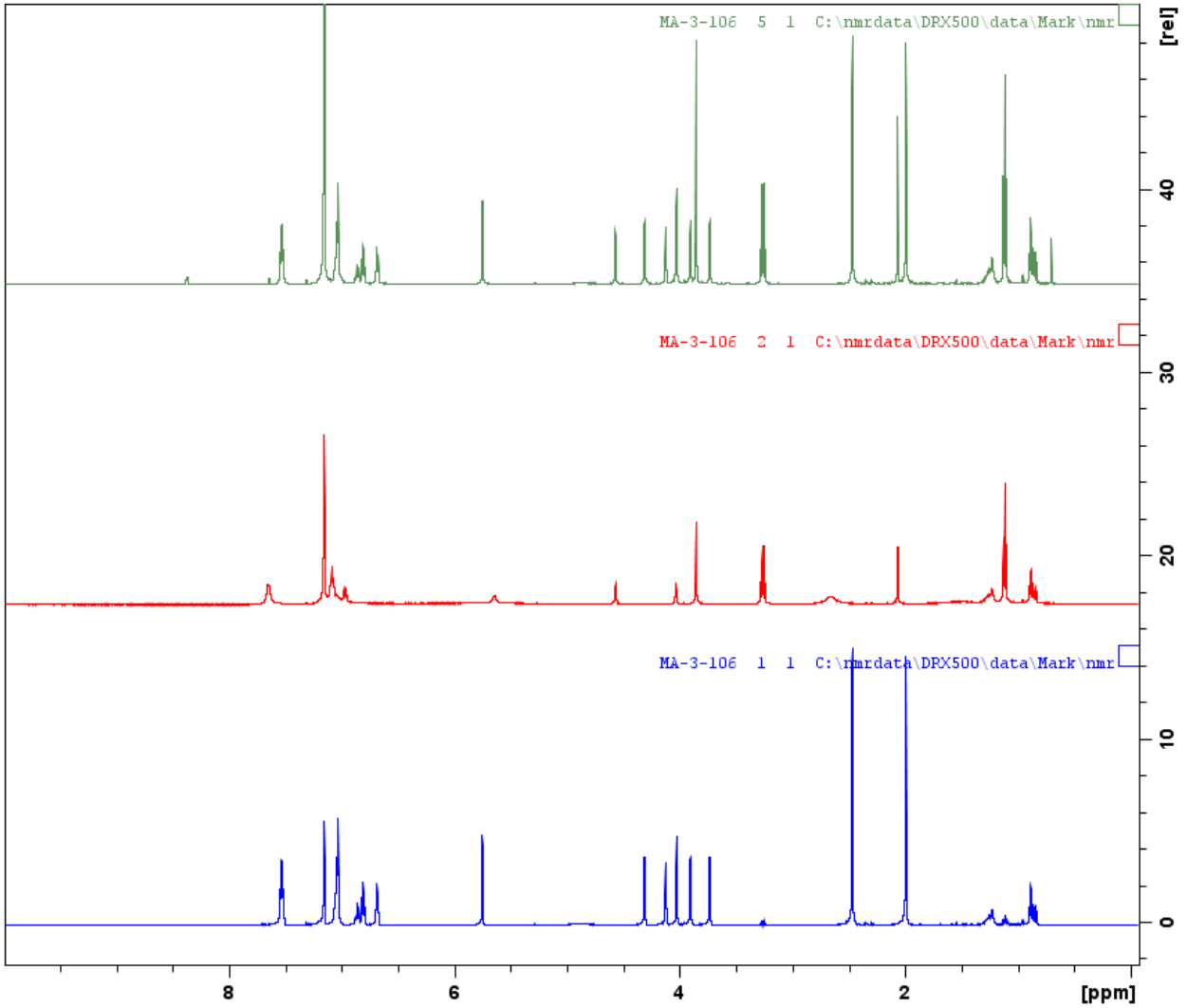

Figure S1. ^{1}H NMR spectra (C_6D_6, 500 MHz, 298 K) of $[(fc^{P,B})Zn(\mu\text{-}OCH_2Ph)]_2$ (bottom), $[(fc^{P,B})Zn(\mu\text{-}OCH_2Ph)]_2$ + $[^{Ac}Fc][BAr^F]$ (middle), $[(fc^{P,B})Zn(\mu\text{-}OCH_2Ph)]_2$ + $[^{Ac}Fc][BAr^F]$ + Cp_2Co (top); related to Equation 1.

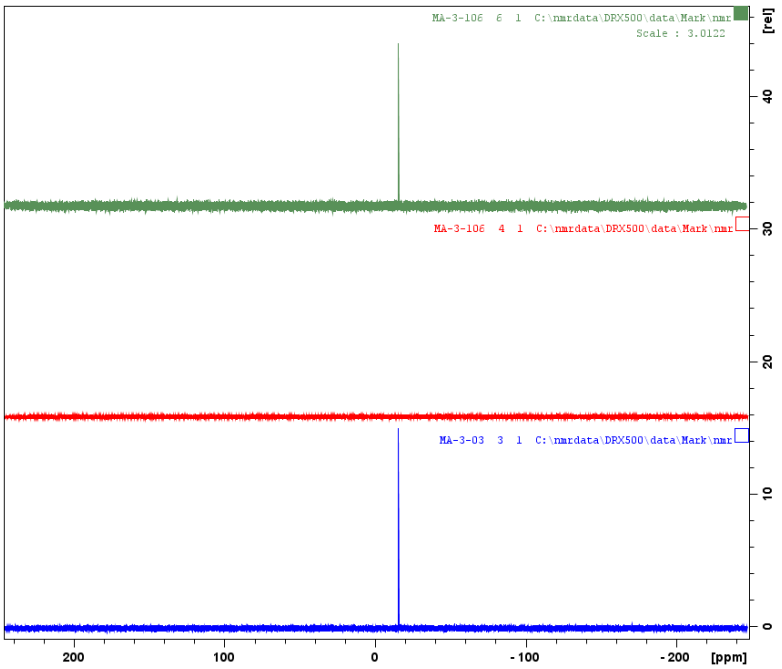

Figure S2. $^{31}P\{^{1}H\}$ NMR spectra (C_6D_6, 202 MHz, 298 K) of $[(fc^{P,B})Zn(\mu\text{-}OCH_2Ph)]_2$ (bottom), $[(fc^{P,B})Zn(\mu\text{-}OCH_2Ph)]_2$ + $[^{Ac}Fc][BAr^F]$ (middle), $[(fc^{P,B})Zn(\mu\text{-}OCH_2Ph)]_2$ + $[^{Ac}Fc][BAr^F]$ + Cp_2Co (top); related to Equation 1.

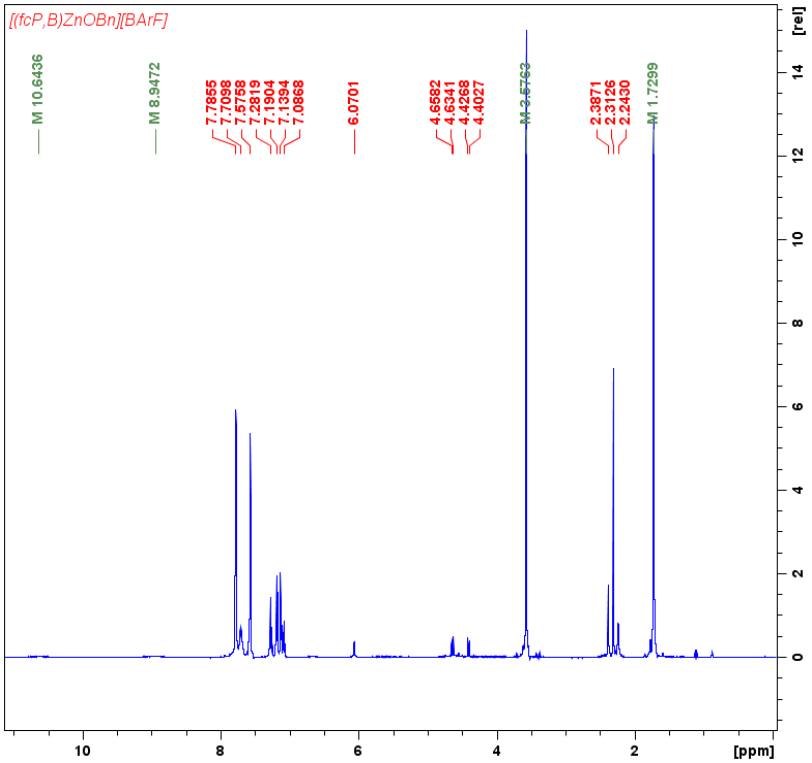

Figure S3. ^{1}H NMR spectrum (THF-d_8, 500 MHz, 298 K) of $[(fc^{P,B})Zn(\mu\text{-}OCH_2Ph)]_2[BAr^F]_2$: δ (ppm) 2.24 (s), 2.39 (s), 4.40 (s), 4.43 (s), 4.63 (s), 4.66 (s), 6.07 (s), 7.09 (t), 7.14 (s), 7.28 (t), 7.58 (s), 7.71 (m), 7.79 (s), 8.95 (br s), 10.64 (br s). Peaks at 2.31 ppm, 7.10 ppm and 7.19 ppm are attributed to residual toluene; related to Equation 1.

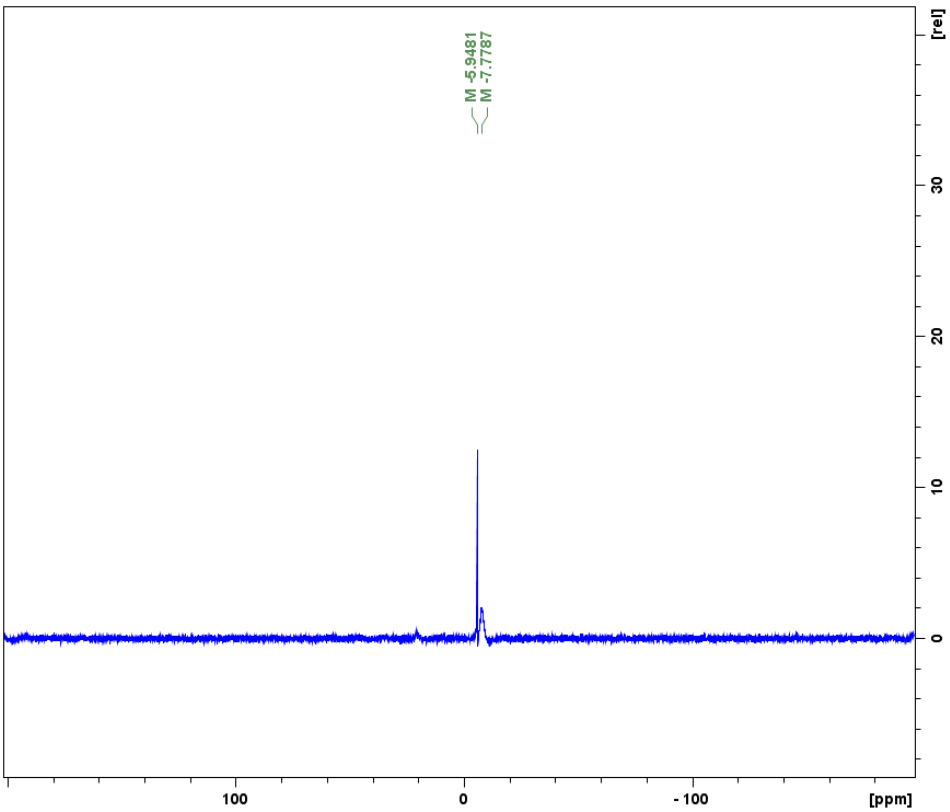

Figure S4. ^{11}B NMR spectrum (THF-d_8, 161 MHz, 298 K) of $[(fc^{P,B})Zn(\mu\text{-}OCH_2Ph)]_2[BAr^F]_2$: δ (ppm) -5.9 (s), -7.8 (br s); related to Equation 1.

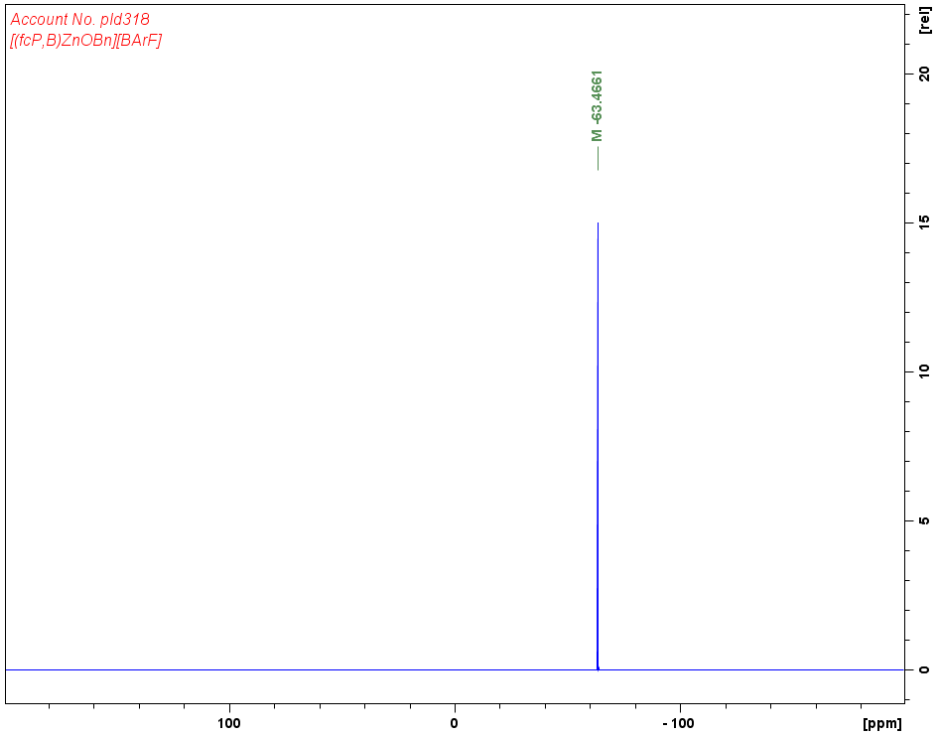

Figure S5. ^{19}F NMR spectrum (THF-d_8, 376 MHz, 298 K) of $[(fc^{P,B})Zn(\mu\text{-}OCH_2Ph)]_2[BAr^F]_2$: δ (ppm) -63.5 (s); related to Equation 1.

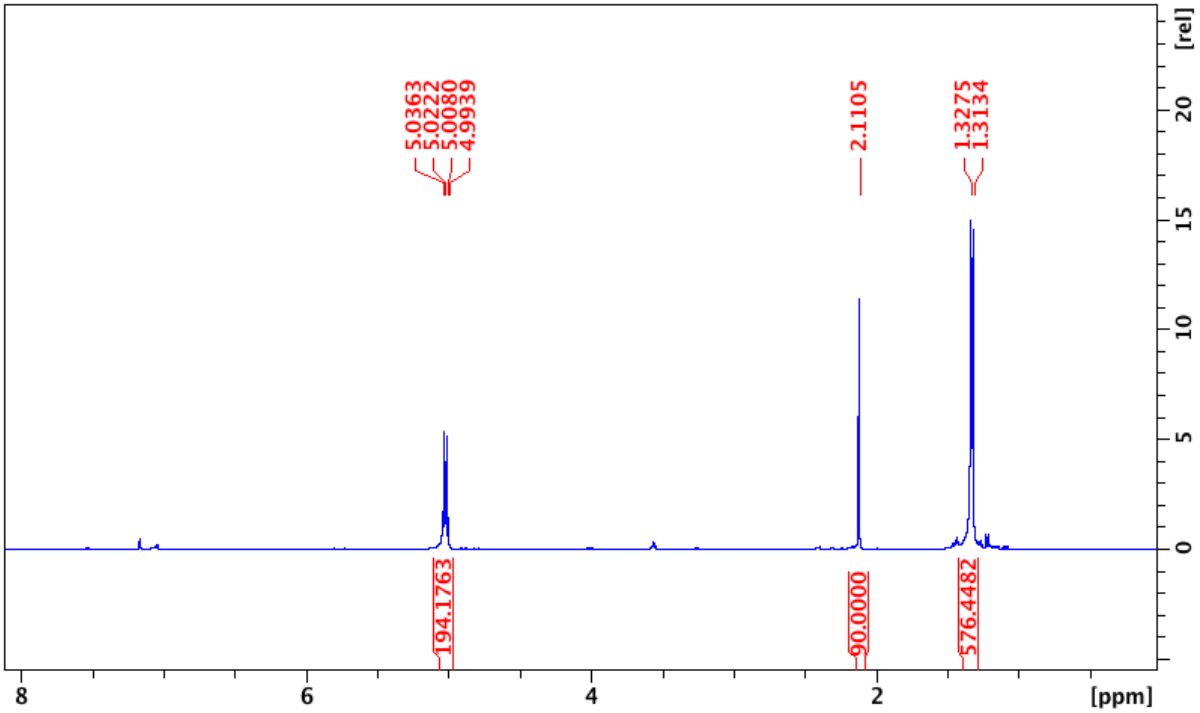

Figure S6. ^{1}H NMR spectrum (C_6D_6, 500 MHz, 298 K) of L-lactide (LA) polymerization. The standard is hexamethylbenzene (HMB). Compound [(fc^{P,B})Zn(μ-OCH$_2$Ph)]$_2$: HMB : LA ratio is 1:10:194. δ (ppm) 1.32 (d, 6H, CHC*H*$_3$ PLA), 2.11 (s, 18H, C*H*$_3$ HMB), 5.01 (q, 2H, C*H*CH$_3$ PLA); related to Table 1, entry 1.

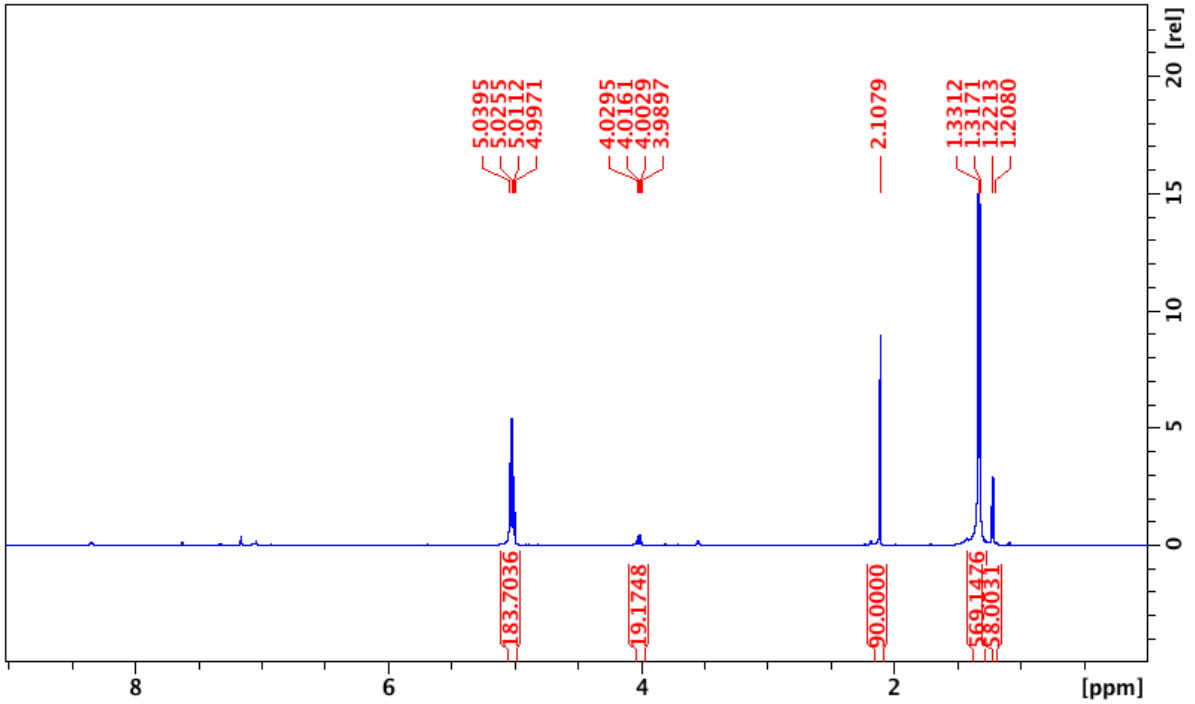

Figure S7. ^{1}H NMR spectrum (C_6D_6, 500 MHz, 298 K) of L-lactide (LA) polymerization. The standard is hexamethylbenzene (HMB). Compound [(fc^{P,B})Zn(μ-OCH$_2$Ph)]$_2$[BAr^{F}]$_2$: HMB : LA ratio is 1:10:184. δ (ppm) 1.21 (d, 6H, CHC*H*$_3$ LA), 1.32 (d, 6H, CHC*H*$_3$ PLA), 2.11 (s, 18H, C*H*$_3$ HMB), 4.01 (q, 2H, C*H*CH$_3$ LA), 5.01 (q, 2H, C*H*CH$_3$ PLA); related to Table 1, entry 2.

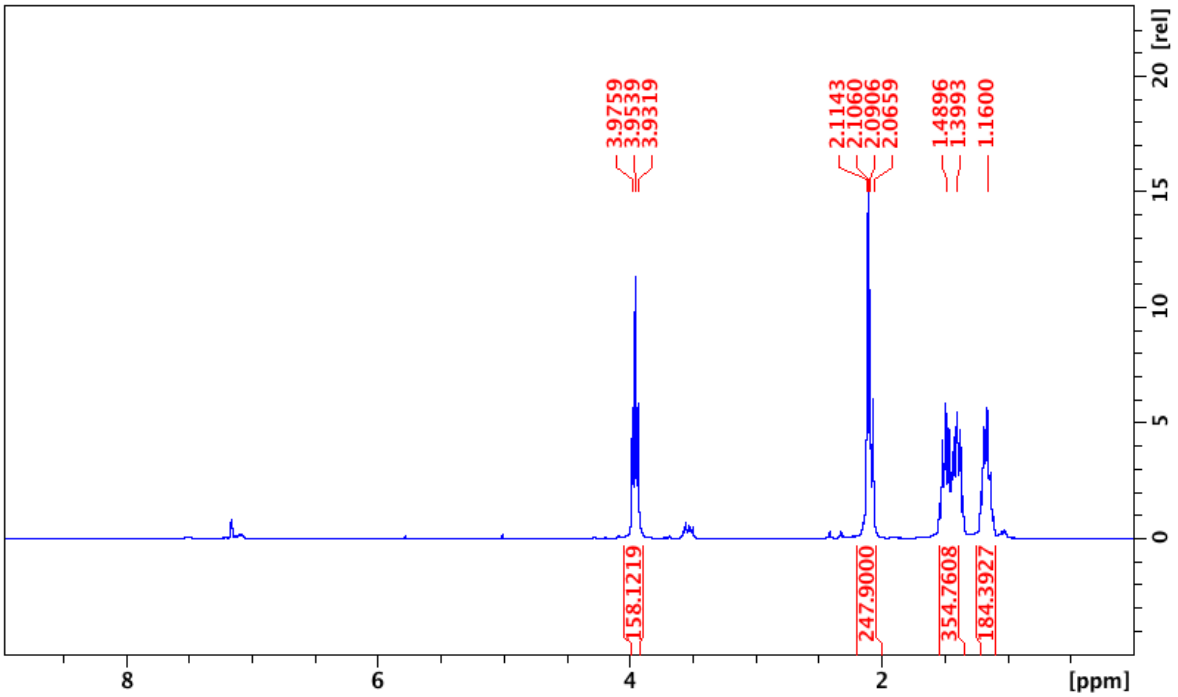

Figure S8. ^{1}H NMR spectrum (C_6D_6, 300 MHz, 298 K) of ε-caprolactone (CL) polymerization. The standard is hexamethylbenzene (HMB). Compound $[(fc^{P,B})Zn(\mu\text{-}OCH_2Ph)]_2$: HMB : CL ratio is 1:10:158. δ (ppm) 1.0–1.6 (6H, C*H*$_2$ PCL), 2.09 (t, 2H, C*H*$_2$ PCL), 2.11 (s, 18H, C*H*$_3$ HMB), 3.95 (t, 2H, C*H*$_2$ PCL); related to Table 1, entry 3.

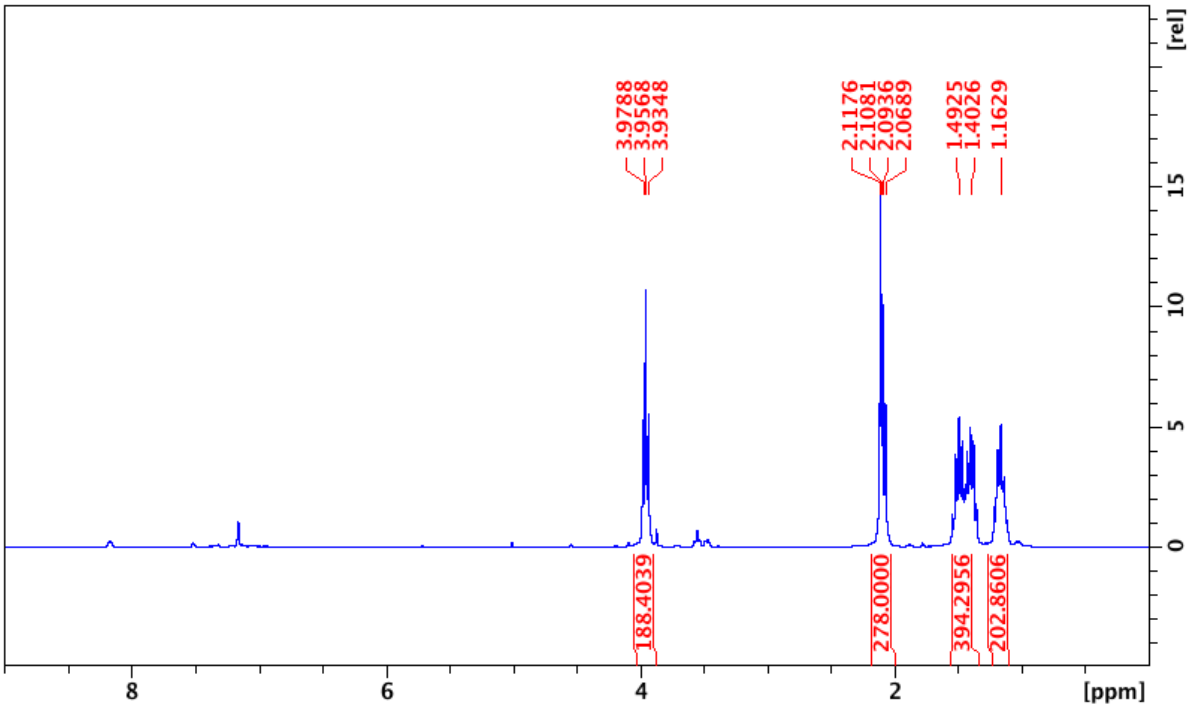

Figure S9. ^{1}H NMR spectrum (C_6D_6, 300 MHz, 298 K) of ε-caprolactone (CL) polymerization. The standard is hexamethylbenzene (HMB). Compound $[(fc^{P,B})Zn(\mu\text{-}OCH_2Ph)]_2[BAr^F]_2$: HMB : CL ratio is 1:10:188. δ (ppm) 1.0–1.6 (6H, C*H*$_2$ PCL), 2.09 (t, 2H, C*H*$_2$ PCL), 2.11 (s, 18H, C*H*$_3$ HMB), 3.95 (t, 2H, C*H*$_2$ PCL); related to Table 1, entry 4.

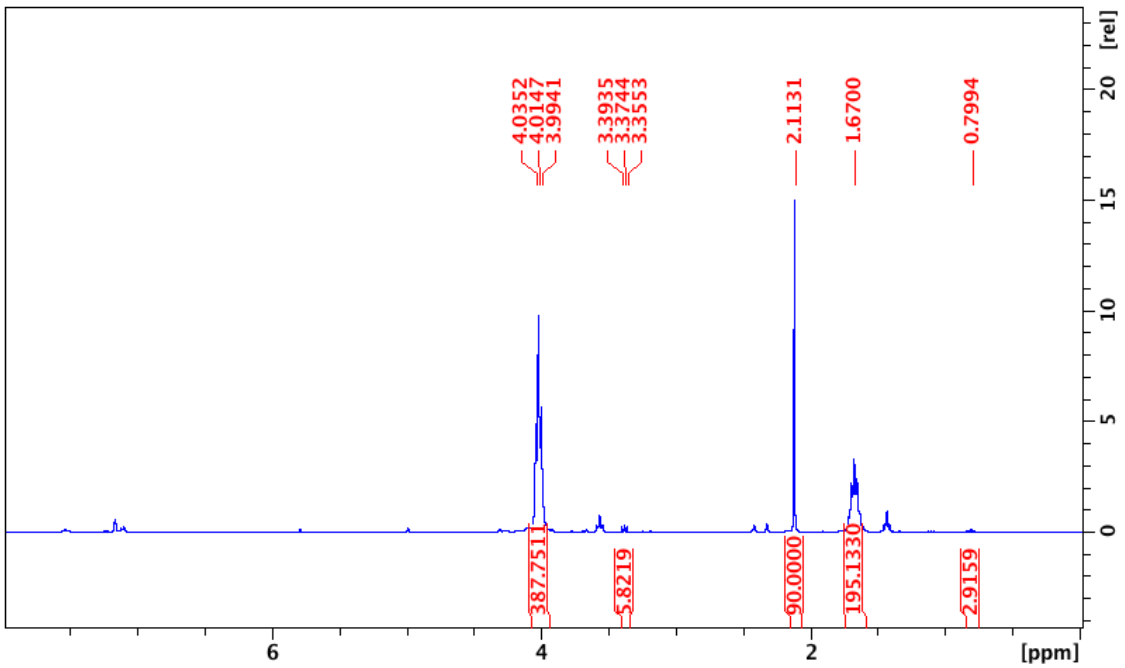

Figure S10. ^{1}H NMR spectrum (C_6D_6, 500 MHz, 298 K) of trimethylene carbonate (TMC) polymerization. The standard is hexamethylbenzene (HMB). Compound [($fc^{P,B}$)Zn(μ-OCH_2Ph)]$_2$: HMB : TMC ratio is 1:10:194. δ (ppm) 0.80 (t, 2H, C*H*$_2$ TMC), 1.67 (t, 2H, C*H*$_2$ PTMC), 2.11 (s, 18H, C*H*$_3$ HMB), 3.37 (t, 4H, C*H*$_2$ TMC), 4.01 (t, 4H, C*H*$_2$ PTMC); related to Table 1, entry 5.

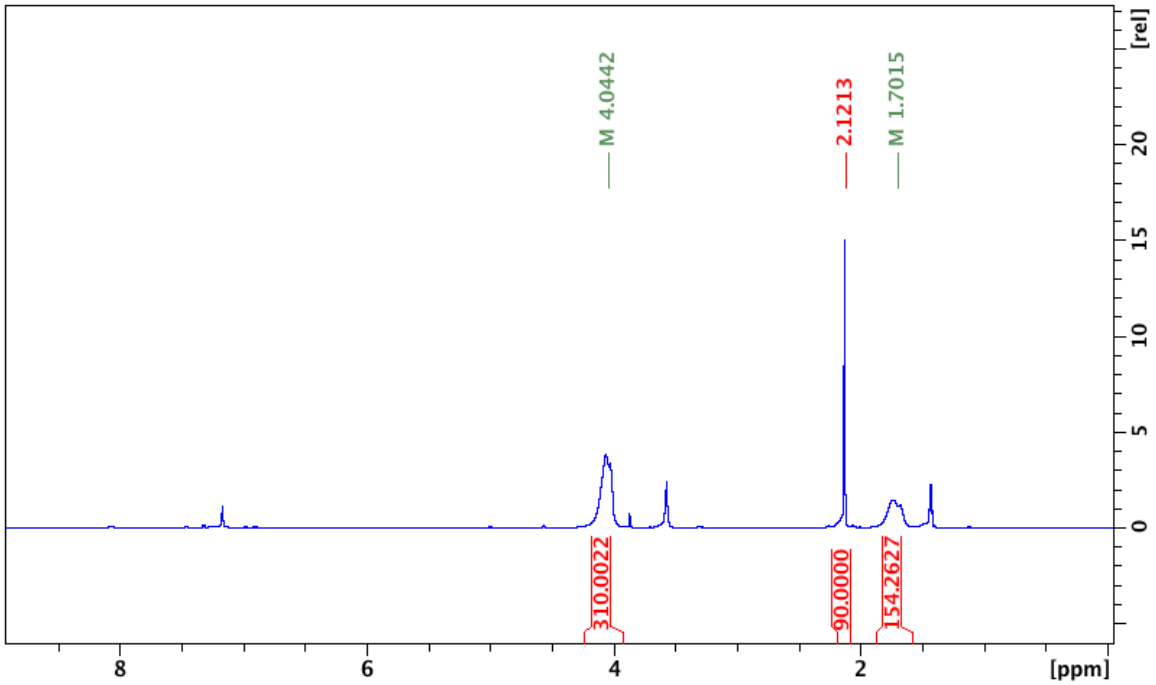

Figure S11. ^{1}H NMR spectrum (C_6D_6, 500 MHz, 298 K) of trimethylene carbonate (TMC) polymerization. The standard is hexamethylbenzene (HMB). Compound [($fc^{P,B}$)Zn(μ-OCH_2Ph)]$_2$[BAr^F]$_2$: HMB : TMC ratio is 1:10:156. δ (ppm) 1.70 (br s, 2H, C*H*$_2$ PTMC), 2.12 (s, 18H, C*H*$_3$ HMB), 4.00 (br s, 4H, C*H*$_2$ PTMC); related to Table 1, entry 6.

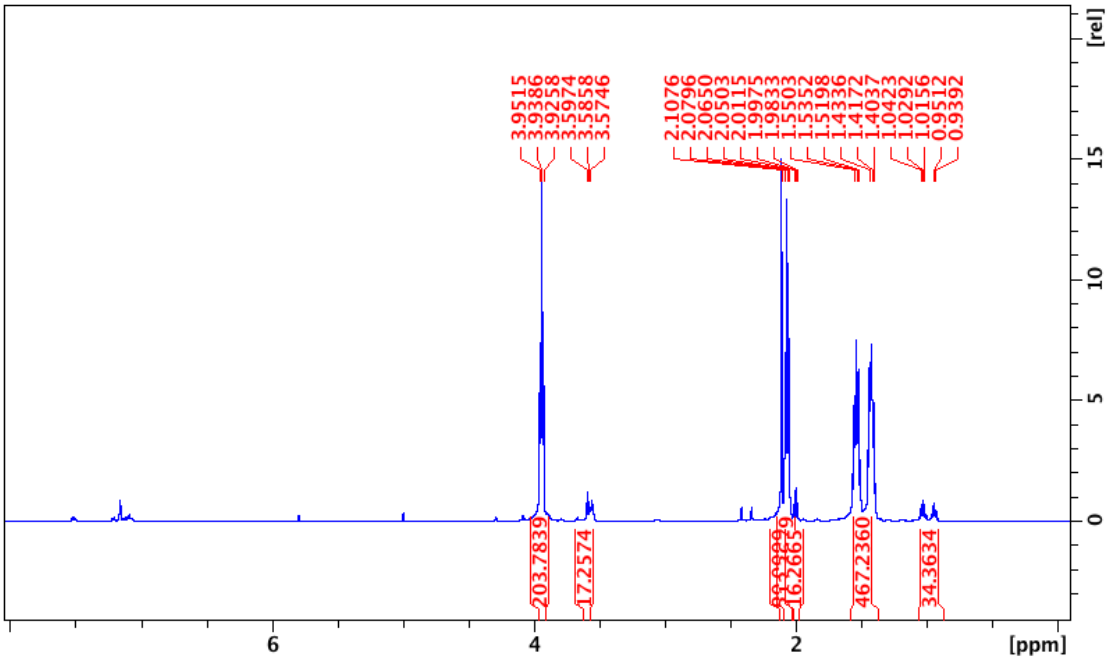

Figure S12. ^{1}H NMR spectrum (C_6D_6, 500 MHz, 298 K) of δ-valerolactone (VL) polymerization. The standard is hexamethylbenzene (HMB). Compound [(fc^{P,B})Zn(μ-OCH$_2$Ph)]$_2$: HMB : VL ratio is 1:10:204. δ (ppm) 0.95 (m, 2H, C*H*$_2$ VL), 1.03 (m, 2H, C*H*$_2$ VL), 1.42 (m, 2H, C*H*$_2$ PVL), 1.54 (m, 2H, C*H*$_2$ PVL), 2.00 (t, 2H, C*H*$_2$ VL), 2.07 (t, 2H, C*H*$_2$ PVL), 2.11 (s, 18H, C*H*$_3$ HMB), 3.59 (t, 2H, C*H*$_2$ VL), 3.94 (t, 2H, C*H*$_2$ PVL); related to Table 1, entry 7.

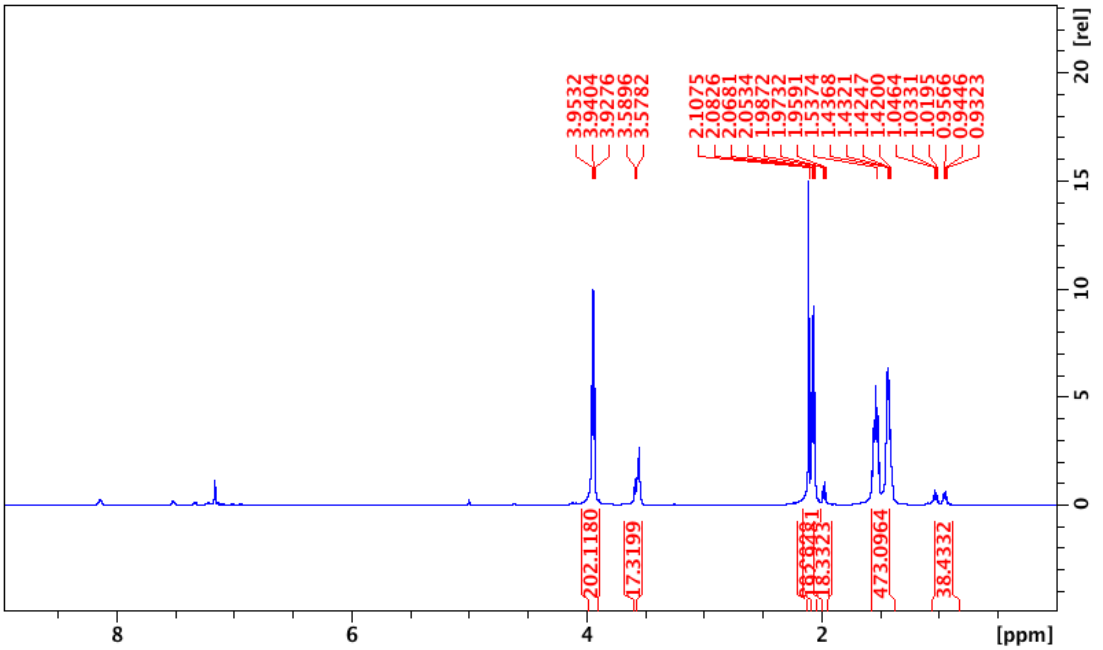

Figure S13. ^{1}H NMR spectrum (C_6D_6, 500 MHz, 298 K) of δ-valerolactone (VL) polymerization. The standard is hexamethylbenzene (HMB). Compound [(fc^{P,B})Zn(μ-OCH$_2$Ph)]$_2$[BAr^{F}]$_2$: HMB : VL ratio is 1:10:202. δ (ppm) 0.95 (m, 2H, C*H*$_2$ VL), 1.03 (m, 2H, C*H*$_2$ VL), 1.42 (m, 2H, C*H*$_2$ PVL), 1.54 (m, 2H, C*H*$_2$ PVL), 2.00 (t, 2H, C*H*$_2$ VL), 2.07 (t, 2H, C*H*$_2$ PVL), 2.11 (s, 18H, C*H*$_3$ HMB), 3.59 (t, 2H, C*H*$_2$ VL), 3.94 (t, 2H, C*H*$_2$ PVL); related to Table 1, entry 8.

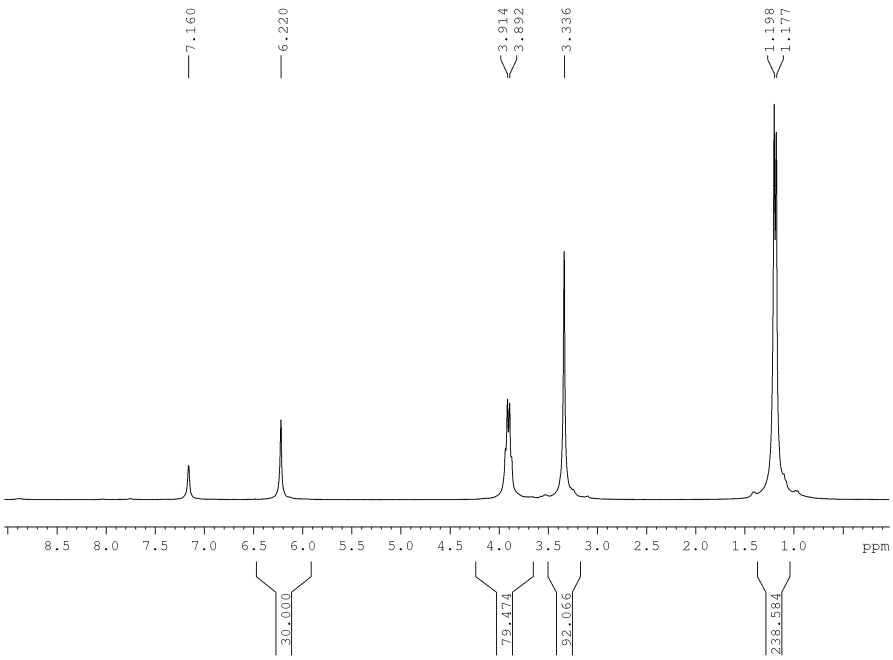

Figure S14. Control experiment of 40 equivalents of L-lactide (LA) with 5 equivalents of [^{Ac}Fc][BAr^{F}] at 70 °C for 3 h; related to Table 1.

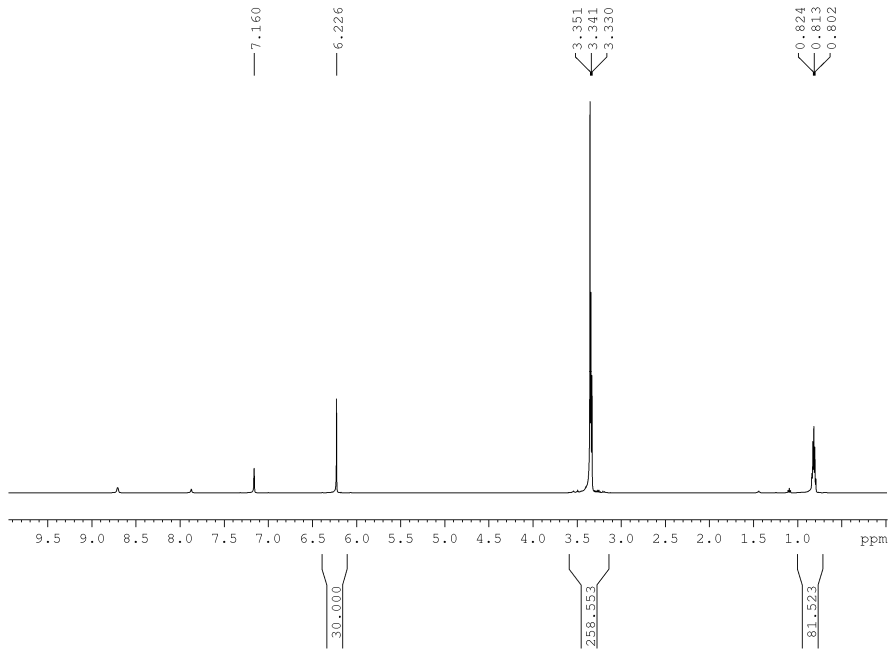

Figure S15. Control experiment of 40 equivalents of trimethylene carbonate (TMC) with 5 equivalents of [^{Ac}Fc][BAr^{F}] at ambient temperature for 2 h; related to Table 1.

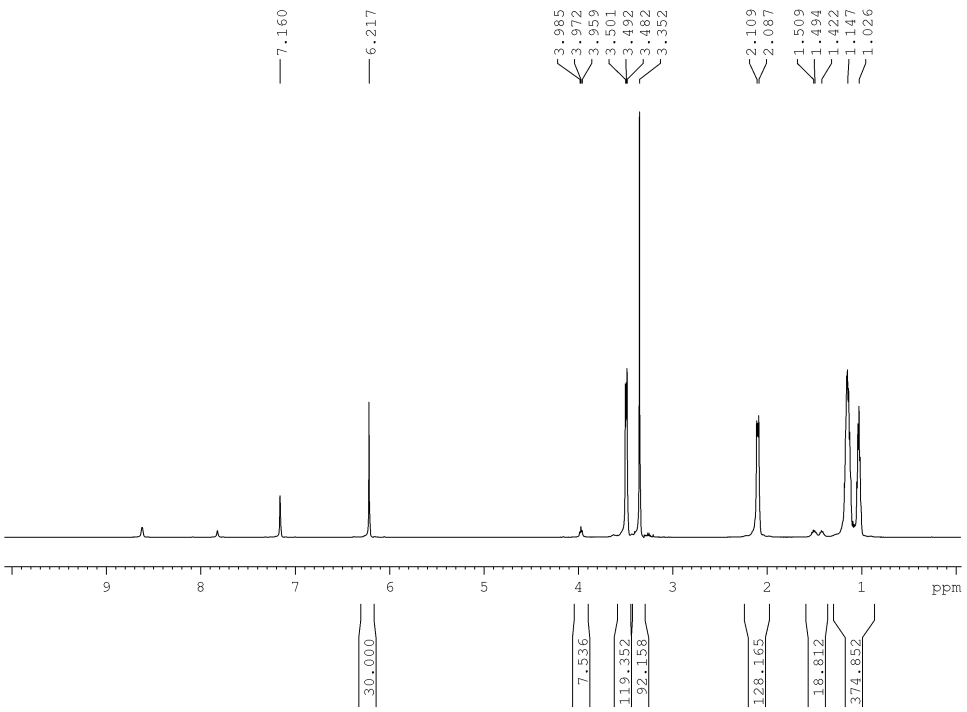

Figure S16. Control experiment of 64 equivalents of ε-caprolactone (CL) with 5 equivalents of [^{Ac}Fc][BAr^{F}] at 70°C for 1 h; related to Table 1.

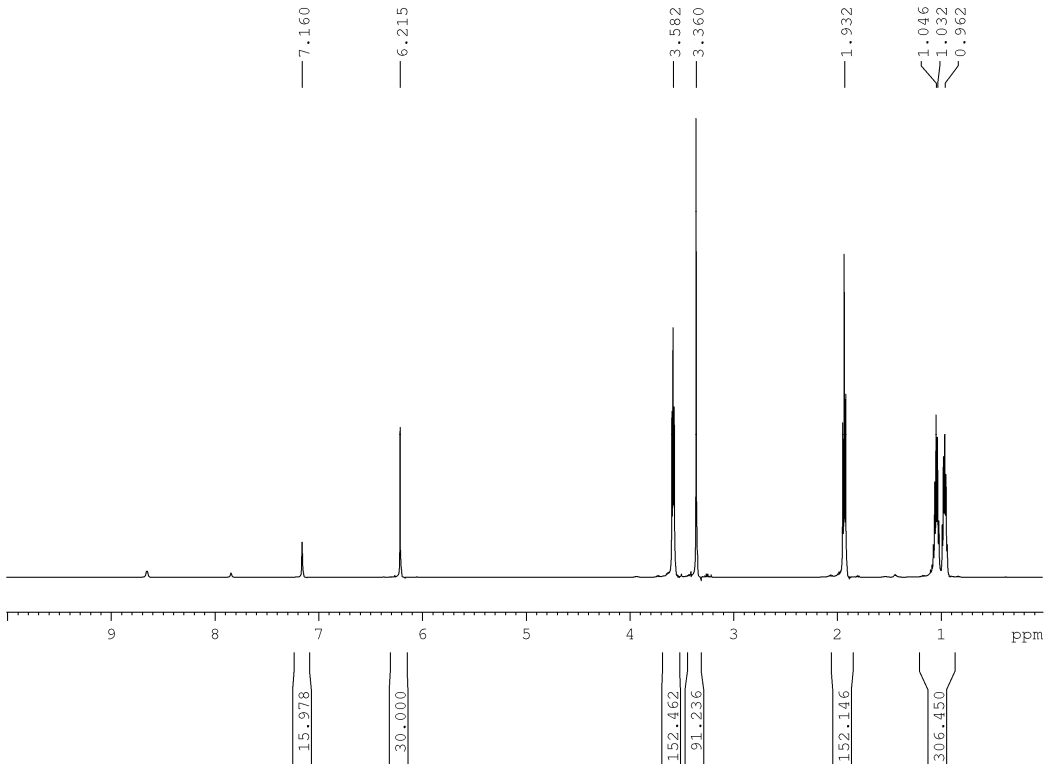

Figure S17. Control experiment of 76 equivalents of δ-valerolactone (VL) with 5 equivalents of [^{Ac}Fc][BAr^{F}] at ambient temperature for 2 h; related to Table 1.

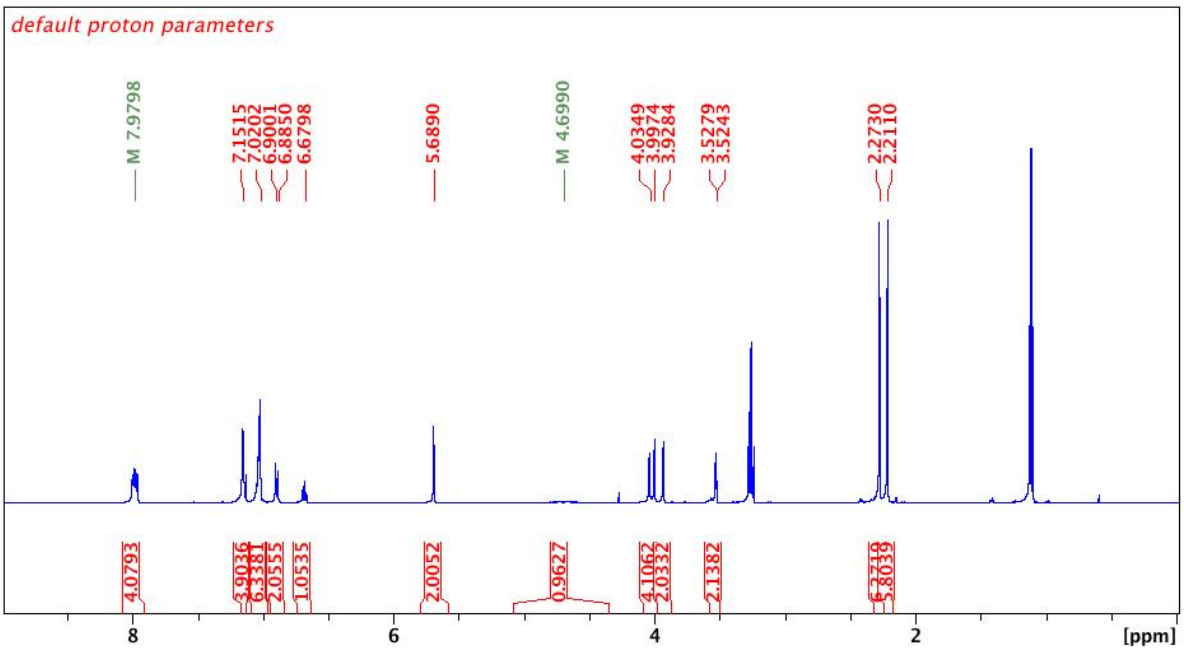

Figure S18. ^{1}H NMR spectrum (C_6D_6, 500 MHz, 298 K) of ($fc^{P,B}$)Zn(OPh): δ (ppm) 2.21 (s, 6H, C*H*$_3$), 2.27 (s, 6H, C*H*$_3$), 3.53 (q, 2H, Cp-*H*), 3.93(t, 2H, Cp-*H*), 4.00 (t, 2H, Cp-*H*), 4.04 (t, 2H, Cp-*H*), 4.70 (br s, 1H, B*H*), 5.69 (s, 2H, C*H*), 6.68 (m, 1H, *p*-Ph), 6.89 (m, 2H, *m*-Ph), 7.02 (m, 6H, *m*-Ph, *p*-Ph), 7.15 (m, 2H, *o*-Ph), 7.98 (m, 4H, *o*-Ph). The peaks at 1.11 and 3.53 are attributed to co-crystallized diethyl ether; related to Equation 2.

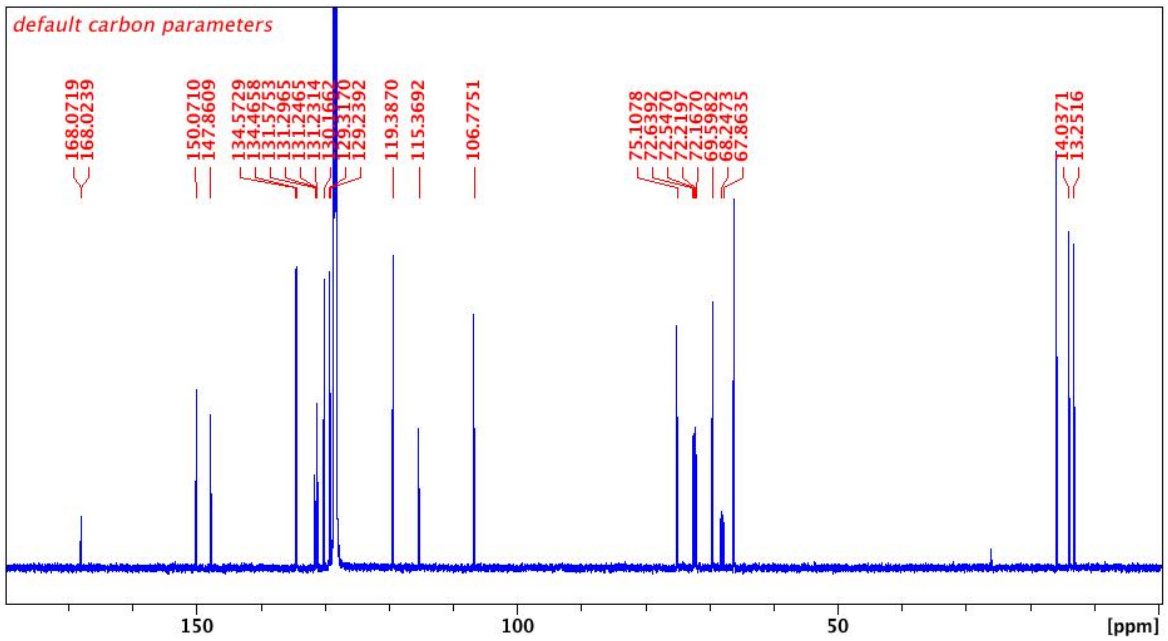

Figure S19. ^{13}C NMR spectrum (C_6D_6, 126 MHz, 298 K) of ($fc^{P,B}$)Zn(OPh): δ (ppm) 13.3 (s, *C*H$_3$), 14.0 (s, *C*H$_3$), 68.1 (d, Cp-*C*), 68.2 (s, Cp-*C*), 69.6 (s, Cp-*C*), 72.2 (d, Cp-*C*), 72.6 (s, Cp-*C*), 75.1 (s, Cp-*C*), 106.8 (s, *C*H), 115.4 (s, aromatic), 119.4 (s, aromatic), 129.3 (d, aromatic), 130.2 (s, aromatic), 131.2 (d, aromatic), 131.4 (d, aromatic), 134.5 (d, aromatic), 147.9 (s, *C*CH$_3$), 150.1 (s, *C*CH$_3$), 168.0 (d, aromatic). The peaks at 15.9 and 66.3 are attributed to co-crystallized diethyl ether; related to Equation 2.

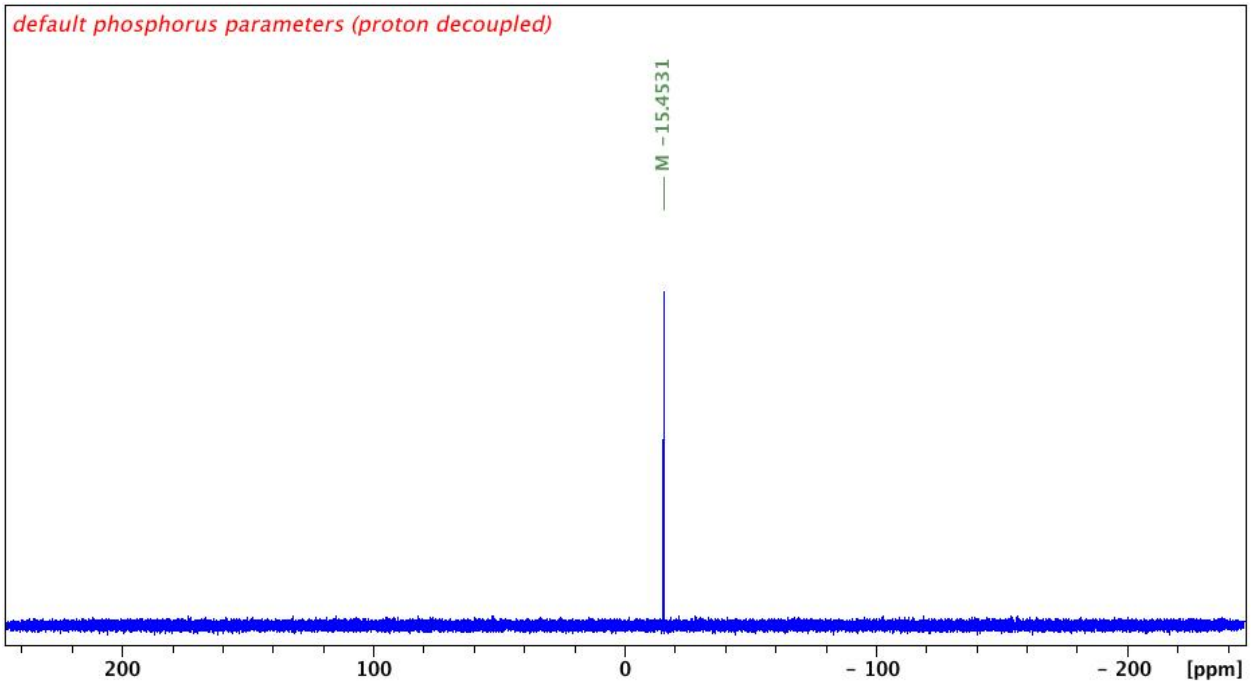

Figure S20. $^{31}P\{^{1}H\}$ NMR spectrum (C_6D_6, 203 MHz, 298 K) of ($fc^{P,B}$)Zn(OPh): δ (ppm) -15.5 (s); related to Equation 2.

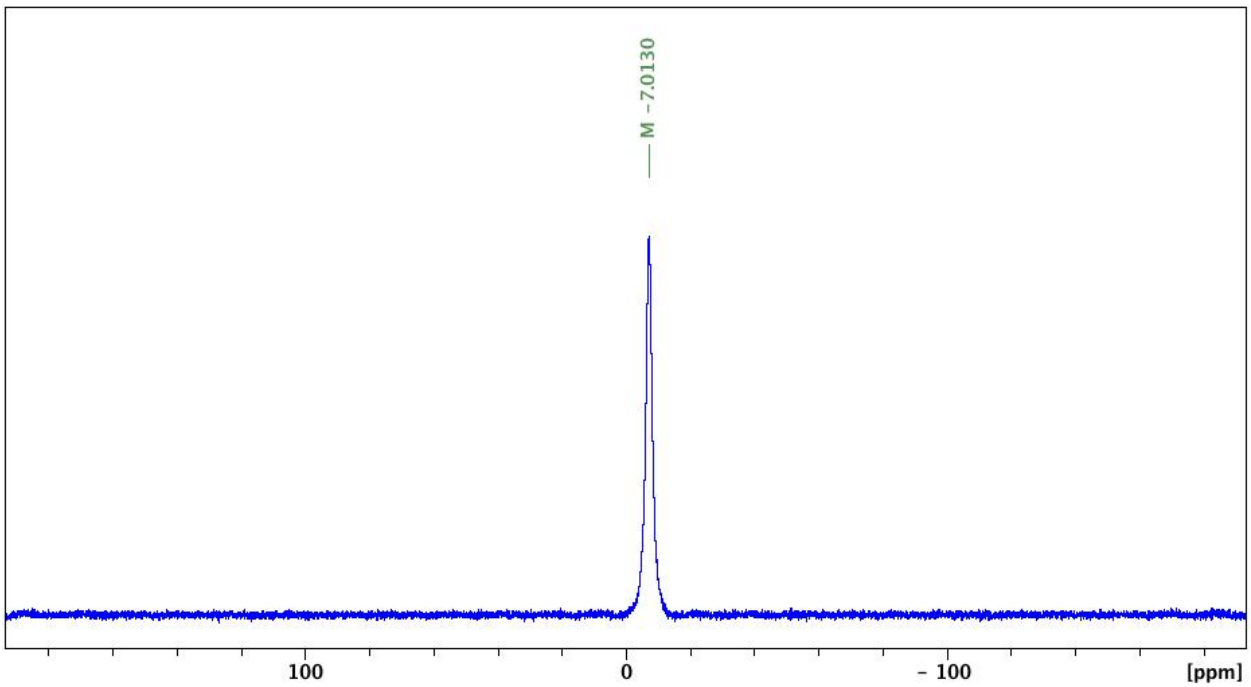

Figure S21. ^{11}B NMR spectrum (C_6D_6, 161 MHz, 298 K) of ($fc^{P,B}$)Zn(OPh): δ (ppm) -7.0 (br s); related to Equation 2.

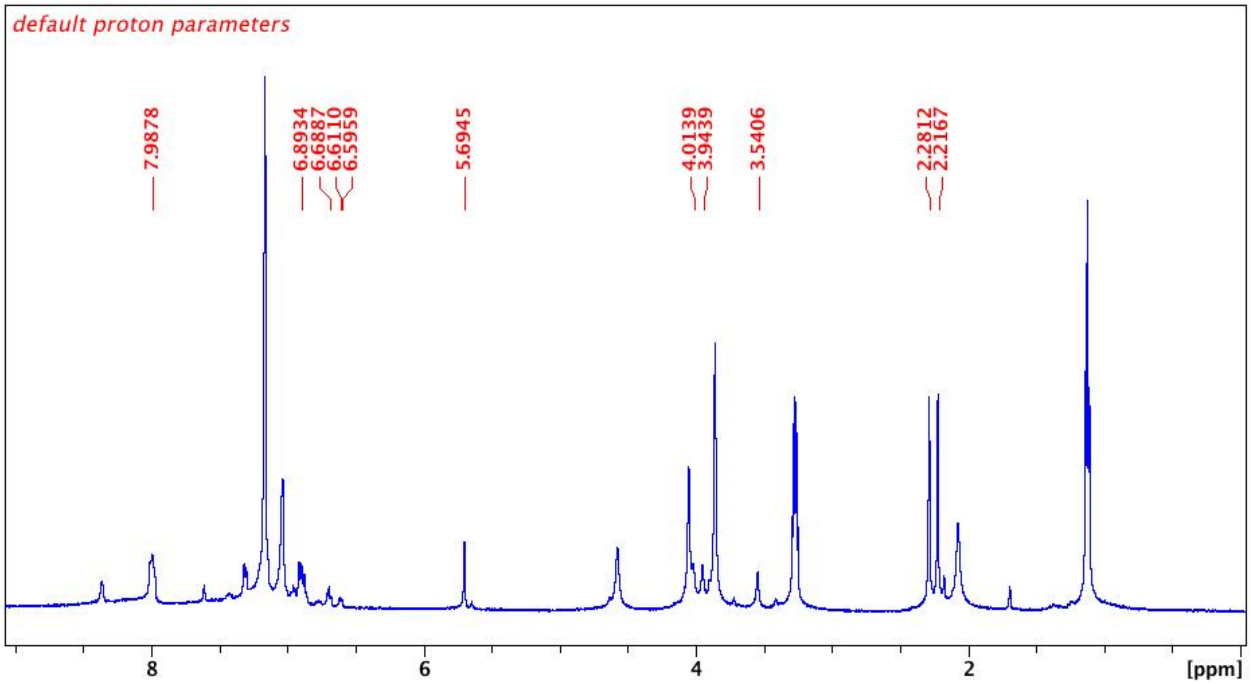

Figure S22. ^{1}H NMR spectrum (C_6D_6, 500 MHz, 298 K) of ($fc^{P,B}$)Zn(OPh) + [^{Ac}Fc][BAr^{F}]; related to Equation 2.

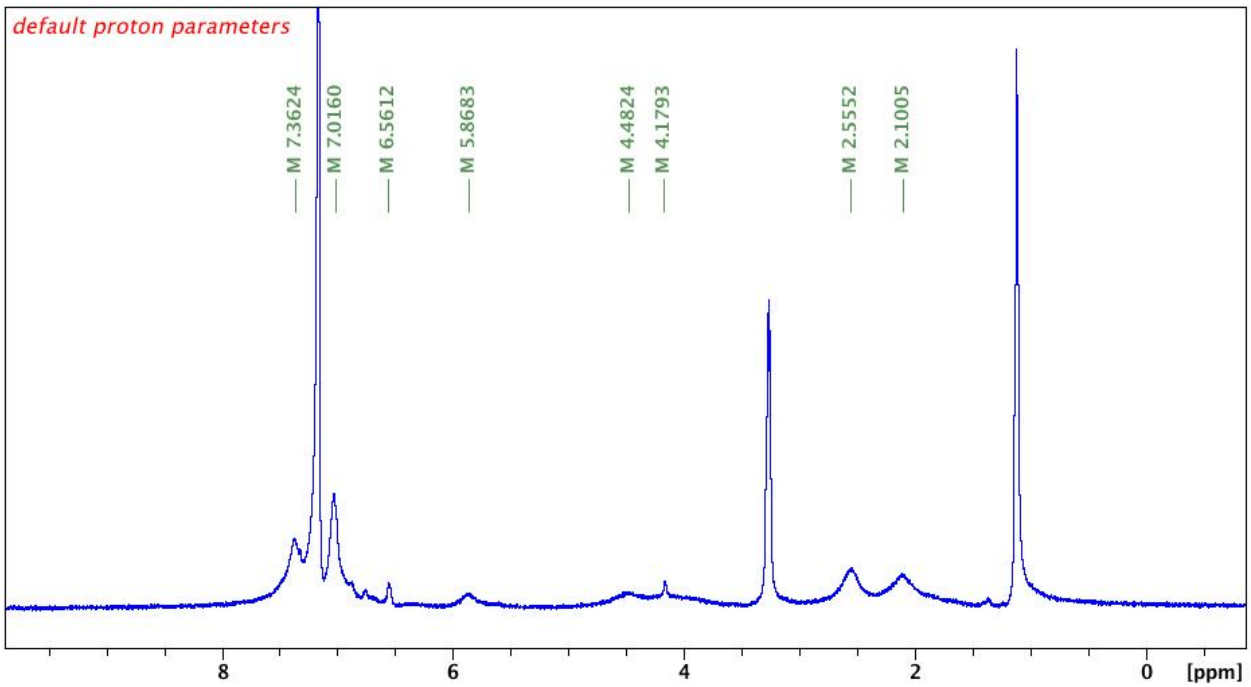

Figure S23. ^{1}H NMR spectrum (C_6D_6, 500 MHz, 298 K) of ($fc^{P,B}$)Zn(OPh) + $AgBF_4$; related to Equation 2.

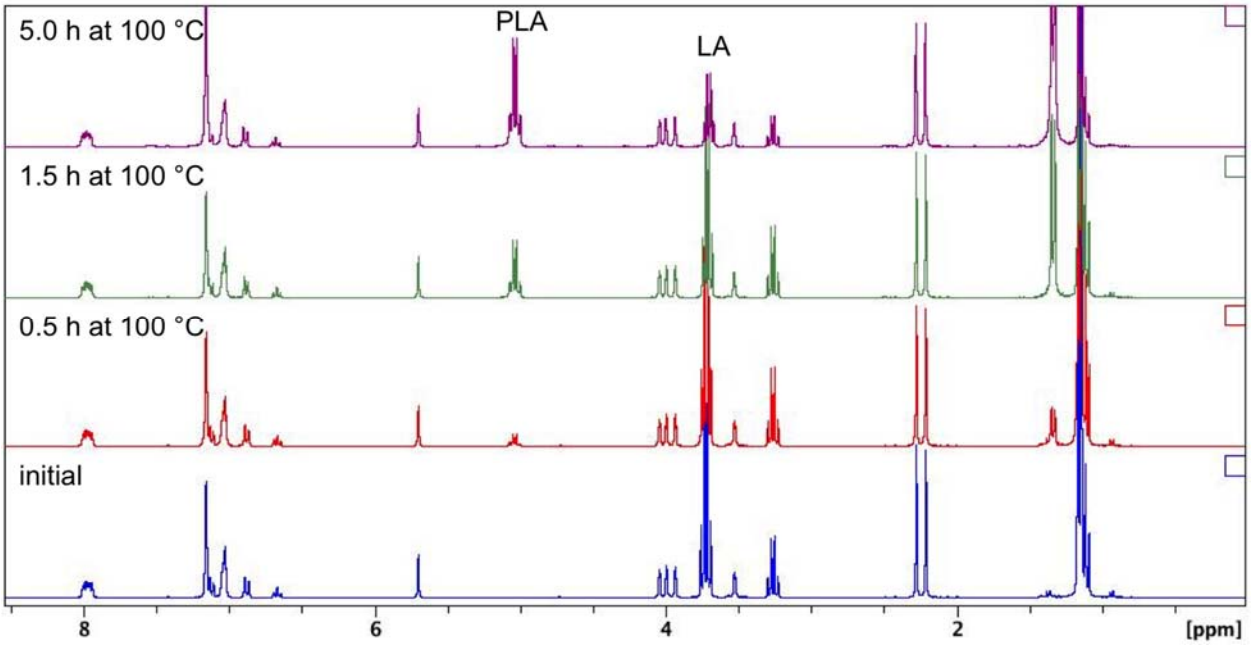

Figure S24. ^{1}H NMR spectra (C_6D_6, 500 MHz, 298 K) of L-lactide polymerization (10 equivalents) in the presence of ($fc^{P,B}$)Zn(OPh); related to Table 1.

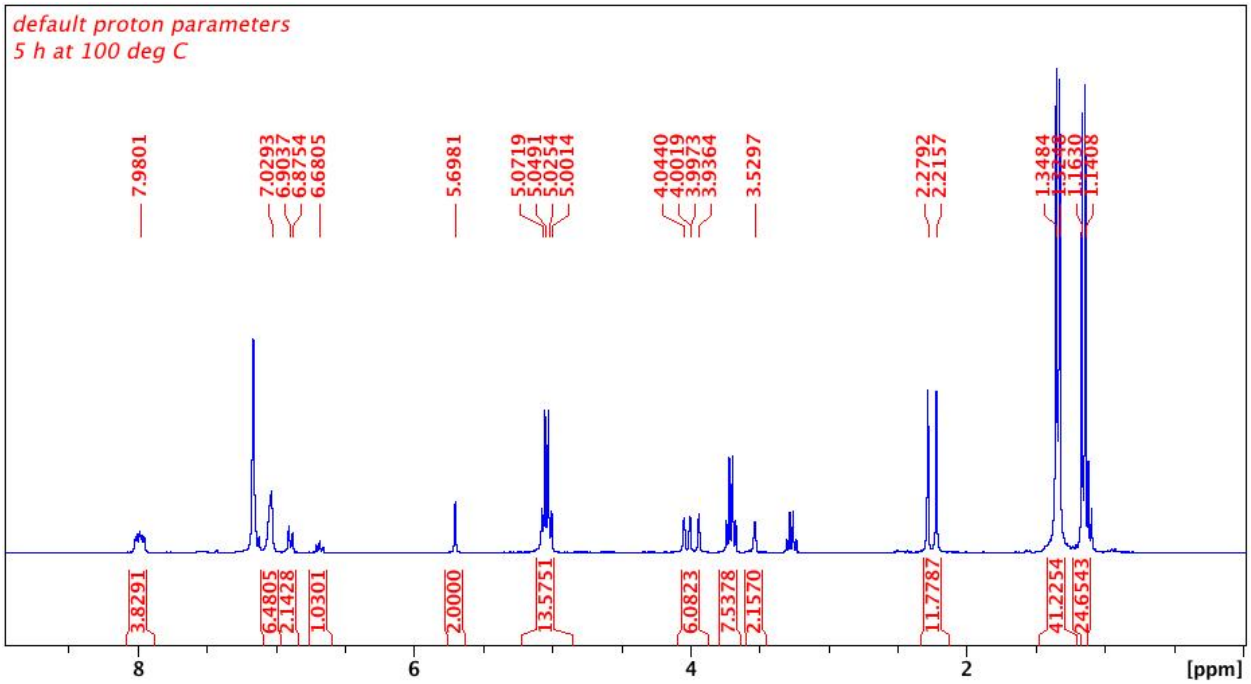

Figure S25. ^{1}H NMR spectrum (C_6D_6, 500 MHz, 298 K) of L-lactide polymerization (10 equivalents) in the presence of ($fc^{P,B}$)Zn(OPh) after 5 h at 100 °C; related to Table 1.

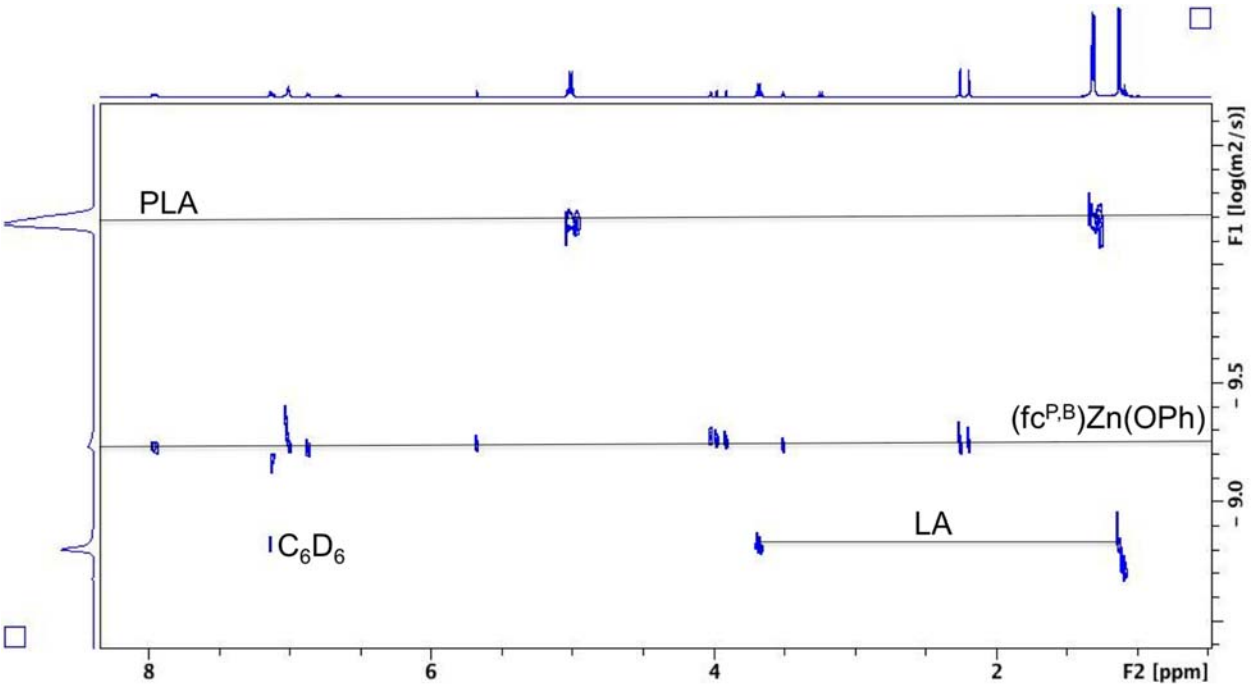

Figure S26. ^{1}H DOSY NMR spectrum (C_6D_6, 500 MHz, 298 K) of L-lactide polymerization (10 equivalents) in the presence of ($fc^{P,B}$)Zn(OPh) after 5 h at 100 °C; related to Table 1.

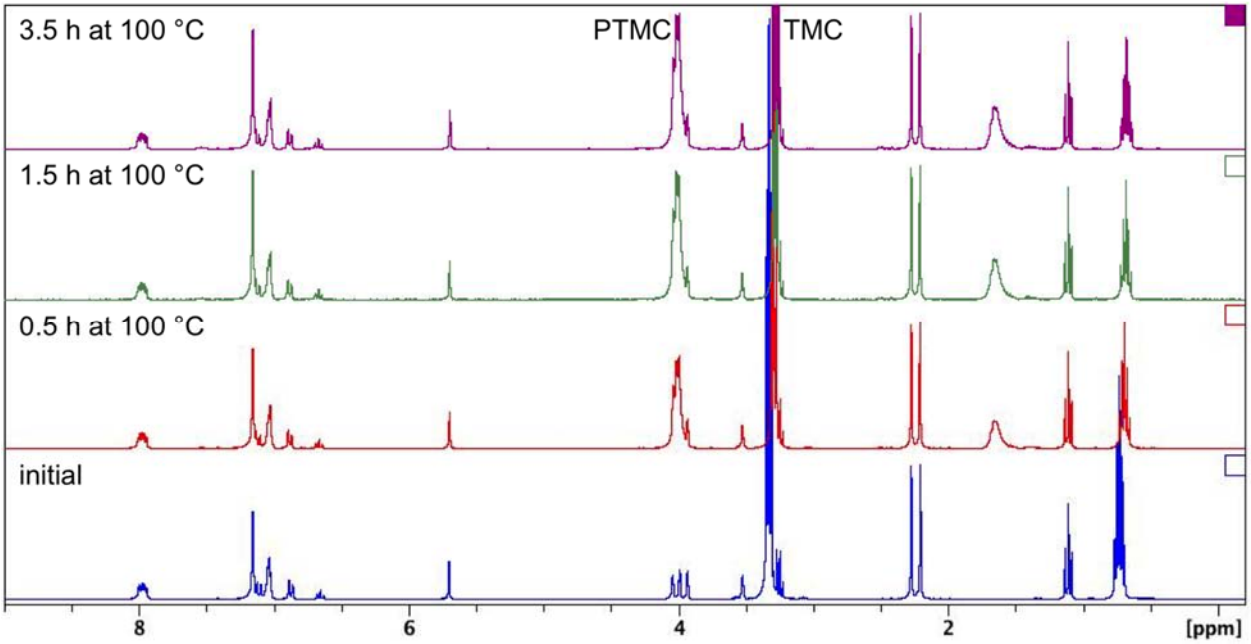

Figure S27. ^{1}H NMR spectra (C_6D_6, 500 MHz, 298 K) of trimethylene carbonate polymerization (13 equivalents) in the presence of ($fc^{P,B}$)Zn(OPh); related to Table 1.

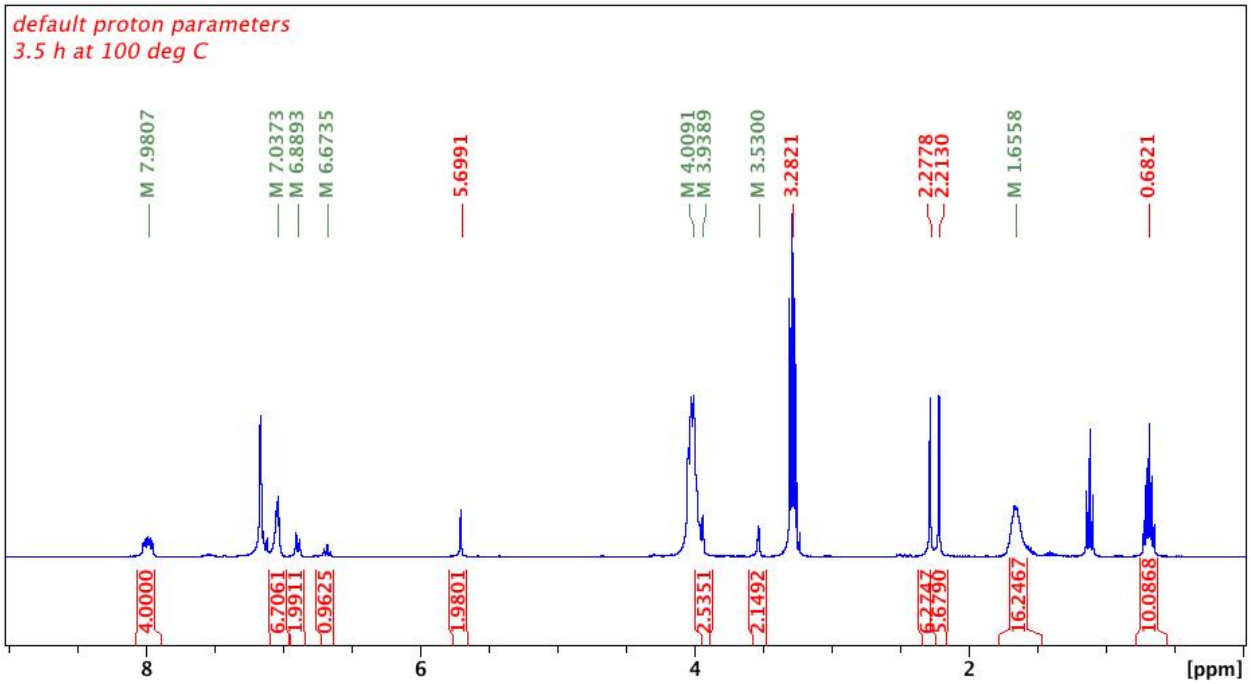

Figure S28. ^{1}H NMR spectrum (C_6D_6, 500 MHz, 298 K) of trimethylene carbonate polymerization (13 equivalents) in the presence of ($fc^{P,B}$)Zn(OPh) after 3.5 h at 100 °C; related to Table 1.

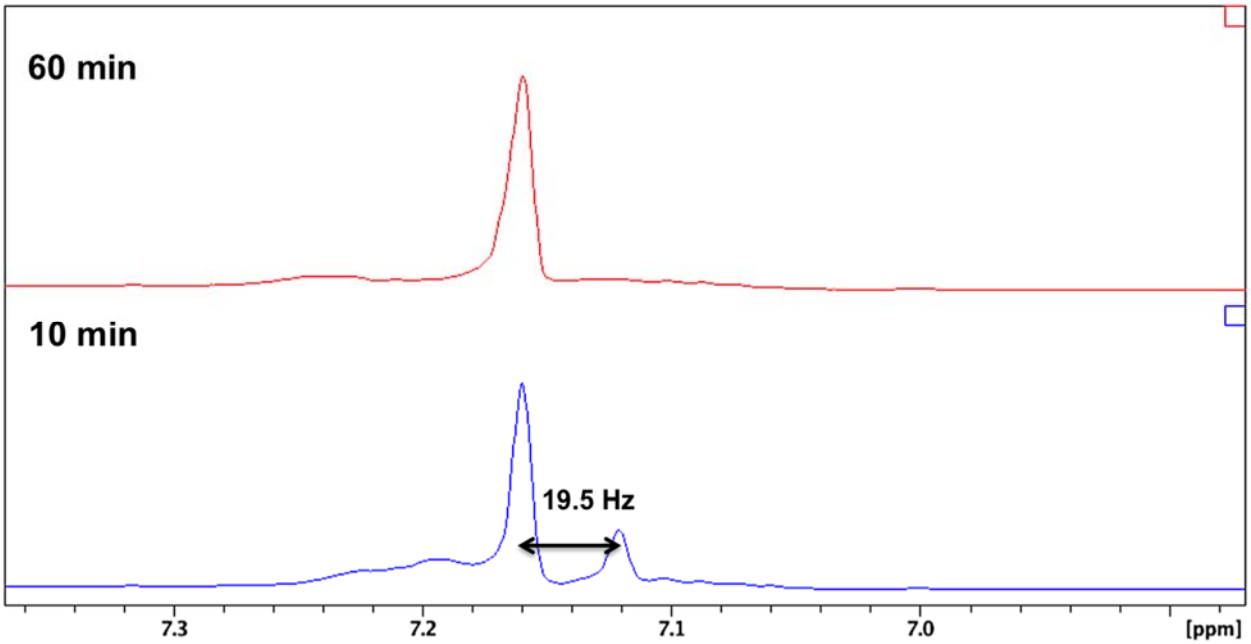

Figure S29. Solution state magnetic susceptibility (C_6D_6, 500 MHz, 298 K) of [($fc^{P,B}$)Zn(μ-OCH_2Ph)]$_2$[BAr^F]$_2$ in the presence of 60 equivalents of trimethylene carbonate. The separation between the solvent peak containing the metal complex and the solvent in the insert is displayed; related to Table 1.

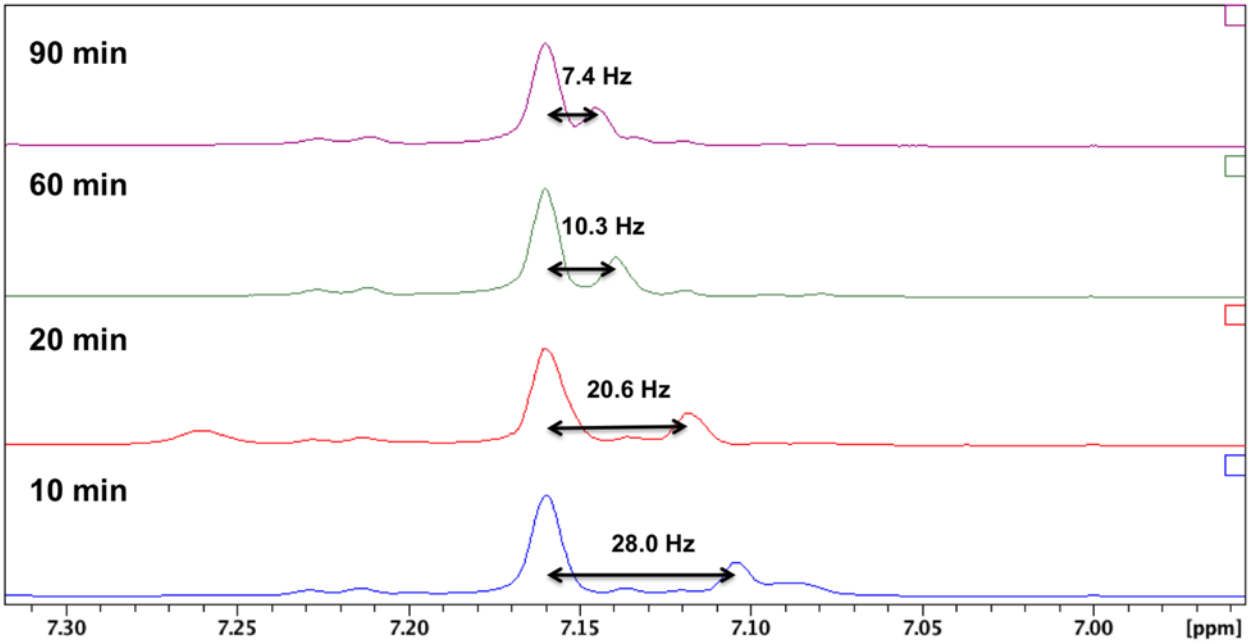

Figure S30. Solution state magnetic susceptibility (C_6D_6, 500 MHz, 298 K) of [(fc^{P,B})Zn(μ-OCH$_2$Ph)]$_2$[BAr^F]$_2$ in the presence of 136 equivalents of δ-valerolactone. The separations between the solvent peak containing the metal complex and the solvent in the insert are displayed; related to Table 1.

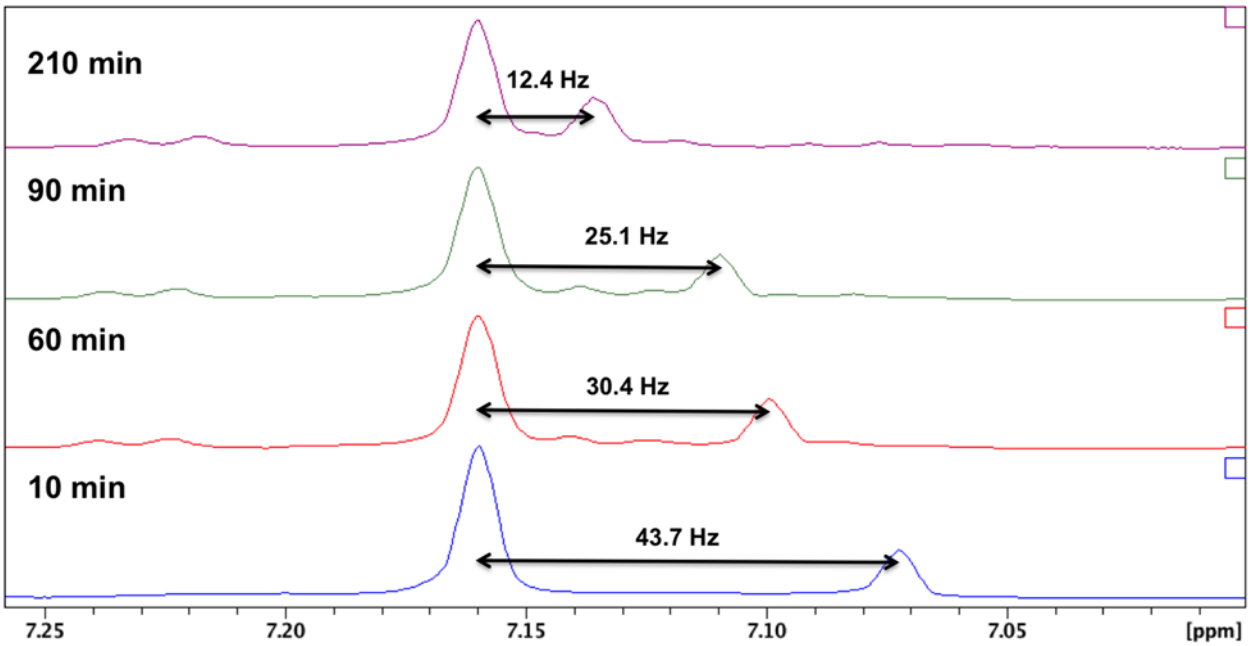

Figure S31. Solution state magnetic susceptibility (C_6D_6, 500 MHz, 298 K) of [(fc^{P,B})Zn(μ-OCH$_2$Ph)]$_2$[BAr^F]$_2$ in the presence of 95 equivalents of ε-caprolactone. The separations between the solvent peak containing the metal complex and the solvent in the insert are displayed; related to Table 1.

Cyclic Voltammetry Data

Calculating i_{pc}/i_{pa}:

$$\frac{i_{pc}}{i_{pa}} = \frac{(i_{pc})_0}{i_{pa}} + 0.485\frac{(i_{sp})_0}{i_{pa}} + 0.086$$

The ratio of the peak currents, i_{pc}/i_{pa}, was determined by the equation above, because the actual baseline for measuring i_{pc} could not be determined in most cases. This was calculated from (a) the uncorrected cathodic peak current, $(i_{pc})_0$, with respect to the zero current baseline and (b) the current at the switching potential $(i_{sp})_0$.

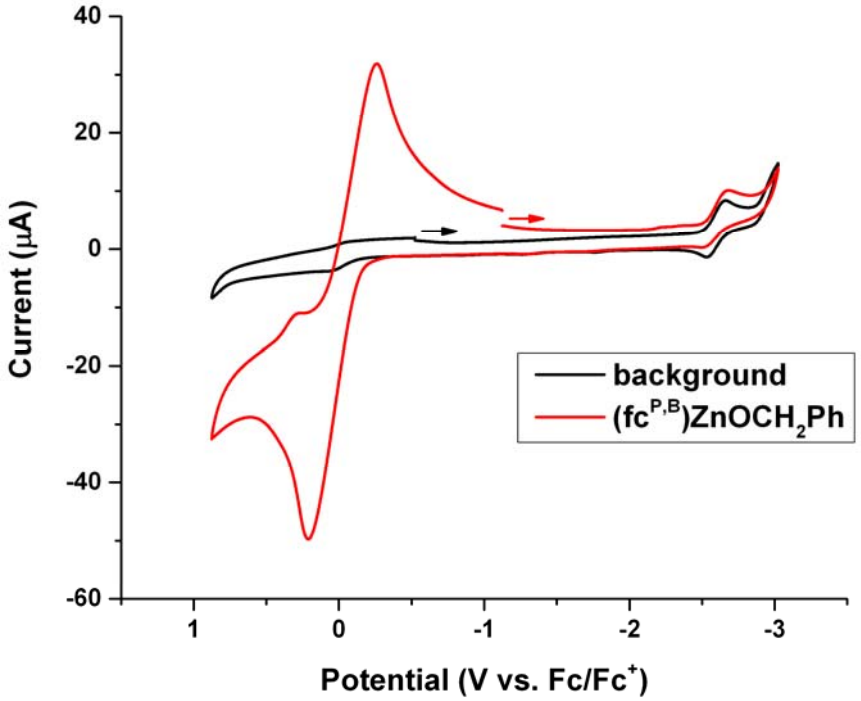

Figure S32. Cyclic voltammograms recorded with a glassy carbon electrode at 100 mV/s in THF, 0.10 M [TBA][PF_6] containing (a) no [($fc^{P,B}$)Zn(μ-OCH_2Ph)]$_2$, (b) 2.5 mM [($fc^{P,B}$)Zn(μ-OCH_2Ph)]$_2$; related to Equation 1.

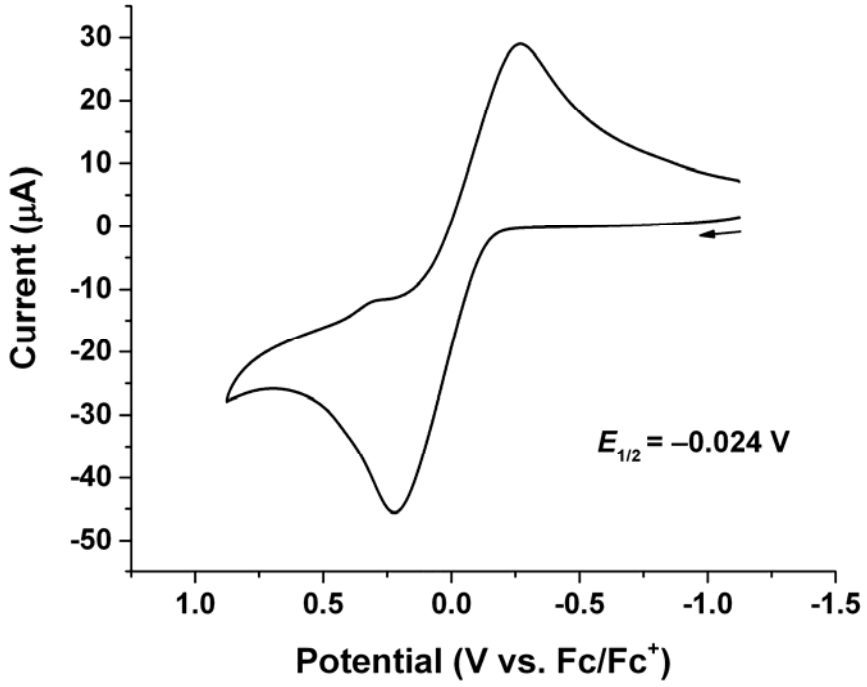

Figure S33. Cyclic voltammogram recorded with a glassy carbon electrode at 100 mV/s in THF, 0.10 M [TBA][PF_6] containing 2.5 mM [($fc^{P,B}$)Zn(μ-OCH_2Ph)]$_2$. $E_{1/2}$ = -0.024 V, i_{pa}/i_{pc} = 1.02; related to Equation 1.

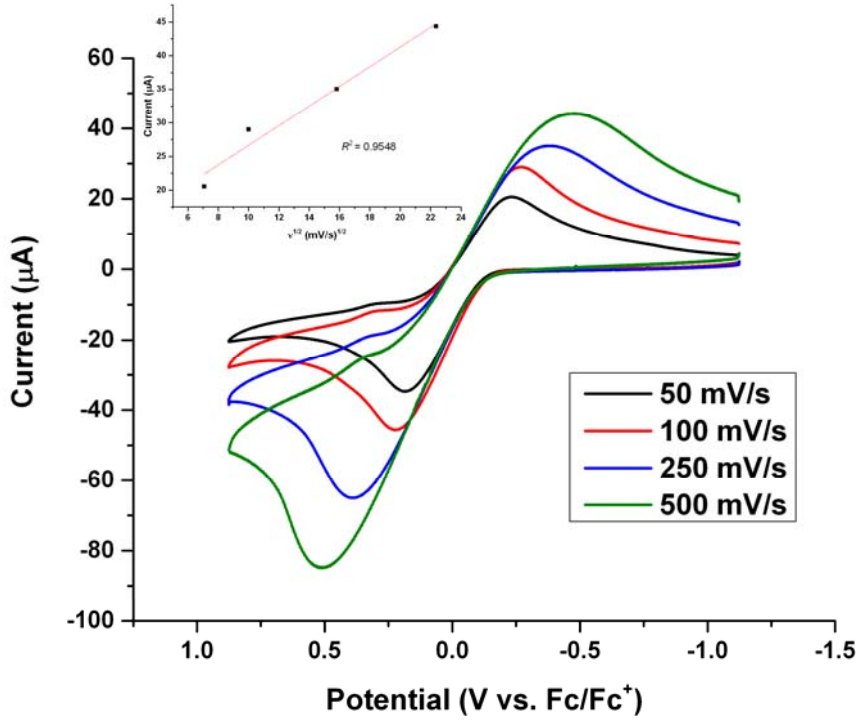

Figure S34. Cyclic voltammograms recorded with a glassy carbon electrode at 50, 100, 250, and 500 mV/s in THF, 0.10 M [TBA][PF_6] containing 2.5 mM [($fc^{P,B}$)Zn(μ-OCH_2Ph)]$_2$; related to Equation 1.

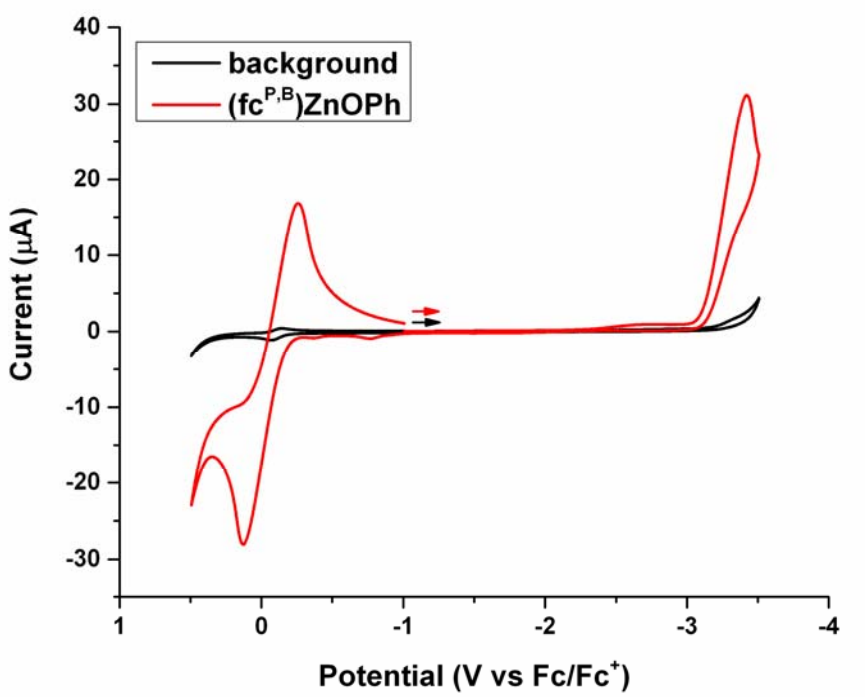

Figure S35. Cyclic voltammograms recorded with a glassy carbon electrode at 100 mV/s in THF, 0.10 M [TBA][PF_6] containing (a) no ($fc^{P,B}$)Zn(OPh), (b) 5.0 mM ($fc^{P,B}$)Zn(OPh); related to Equation 2.

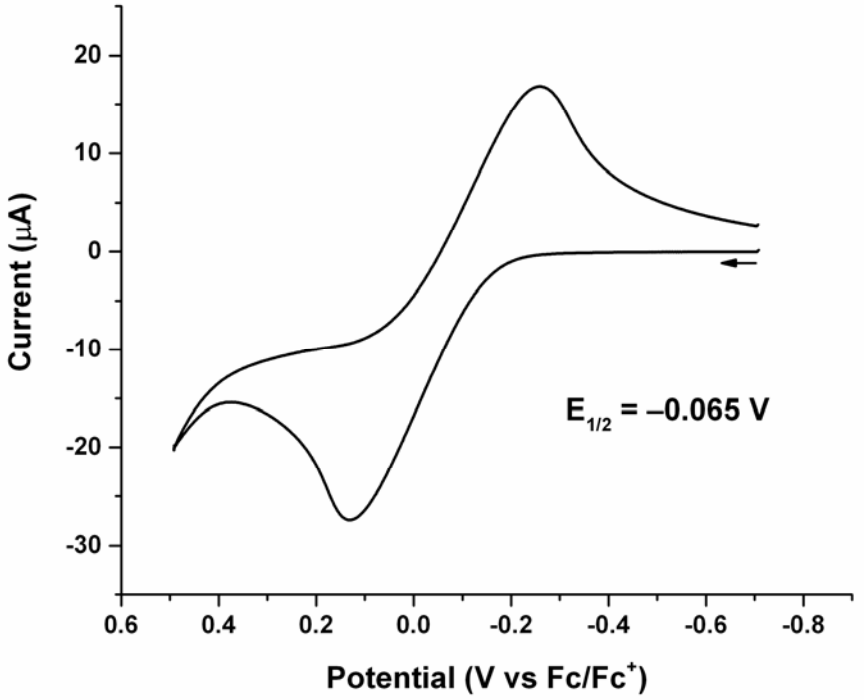

Figure S36. Cyclic voltammogram recorded with a glassy carbon electrode at 100 mV/s in THF, 0.10 M [TBA][PF_6] containing 5.0 mM ($fc^{P,B}$)Zn(OPh). $E_{1/2}$ = -0.065 V, i_{pa}/i_{pc} = 1.06; related to Equation 2.

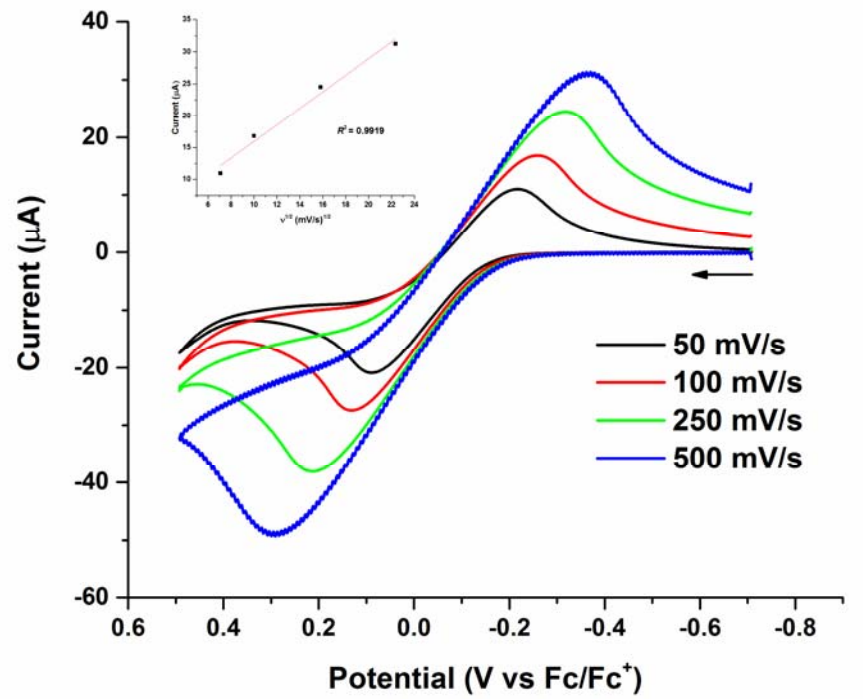

Figure S37. Cyclic voltammograms recorded with a glassy carbon electrode at 50, 100, 250, and 500 mV/s in THF, 0.10 M [TBA][PF_6] containing 5.0 mM ($fc^{P,B}$)Zn(OPh); related to Equation 2.

X-ray Crystallographic Data

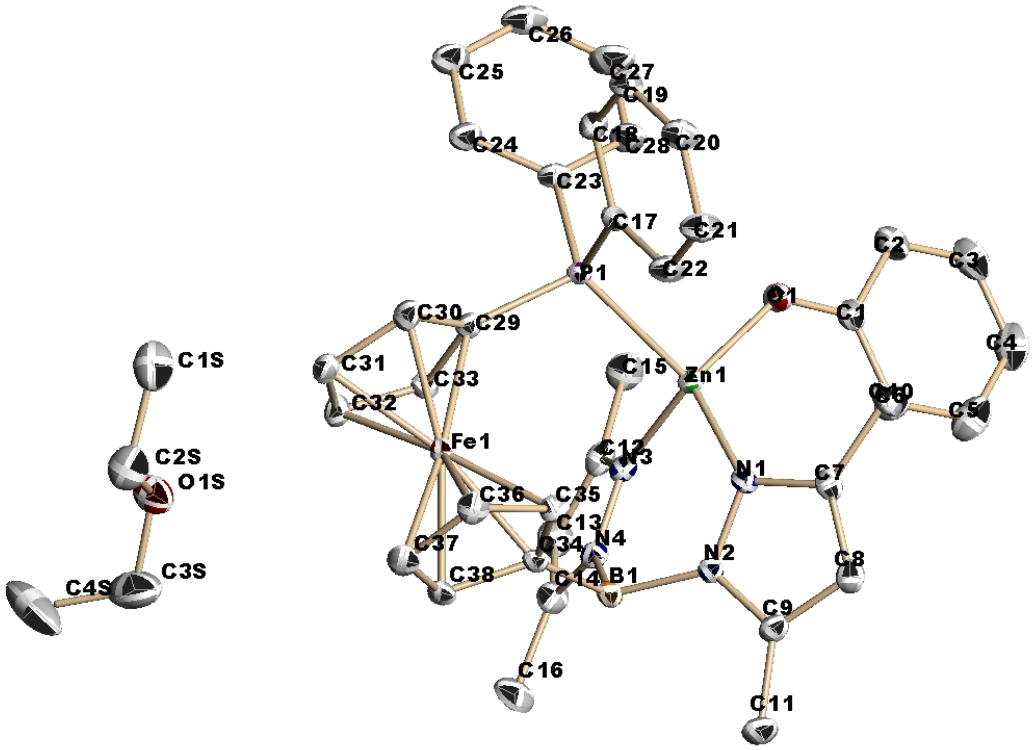

Figure S38. Molecular structure drawing of ($fc^{P,B}$)Zn(OPh) with thermal ellipsoids at 50% probability; hydrogen atoms are omitted for clarity; related to Figure 4.

Crystal data for $C_{42}H_{48}BFeN_4O_2PZn$; $M_r = 803.84$; Monoclinic; space group P21/n; $a = 12.2440(9)$ Å; $b = 14.1412(11)$ Å; $c = 22.6967(17)$ Å; $\alpha = 90°$; $\beta = 94.557(1)°$; $\gamma = 90°$; $V = 3917.4(5)$ Å^3; $Z = 4$; $T = 100(2)$ K; $\lambda = 0.71073$ Å; $\mu = 1.064$ mm^{-1}; $d_{calc} = 1.363$ g·cm^{-3}; 50393 reflections collected; 9606 unique ($R_{int} = 0.0324$); giving $R_1 = 0.0508$, $wR_2 = 0.0924$ for all 9606 data. Residual electron density (e$^-$·Å^{-3}) max/min: 0.63/-0.58.

Size Exclusion Chromatography

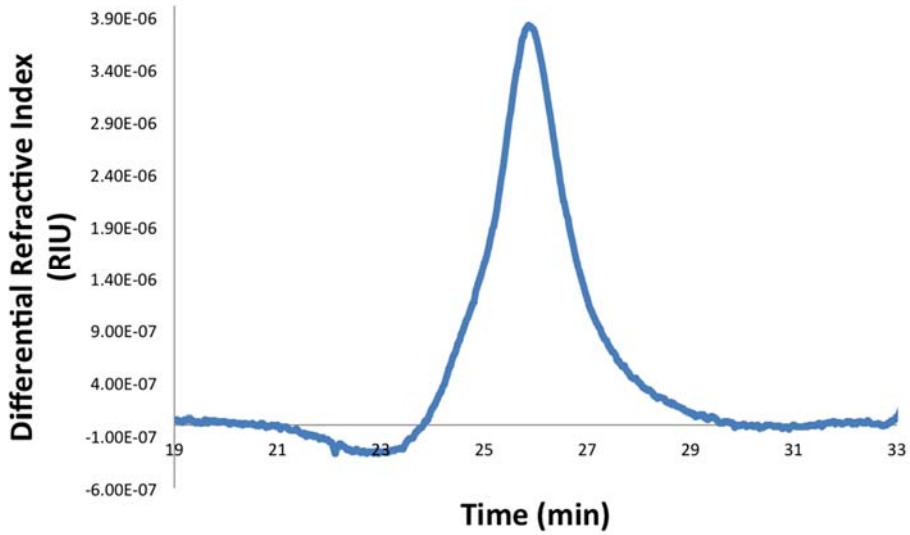

Figure S39. Polymerization of 194 equivalents of L-lactide by compound [(fc^{P,B})Zn(μ-OCH$_2$Ph)]$_2$; M_n = 13,800; $Đ$ = 1.14; related to Table 1, entry 1.

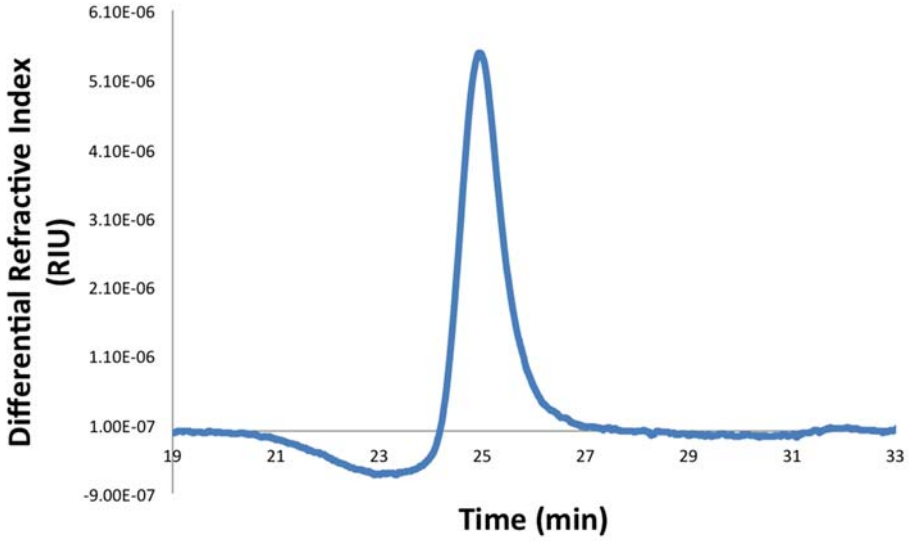

Figure S40. Polymerization of 184 equivalents of L-lactide by compound [(fc^{P,B})Zn(μ-OCH$_2$Ph)]$_2$[BAr^F]$_2$; M_n = 13,500; $Đ$ = 1.03; related to Table 1, entry 2.

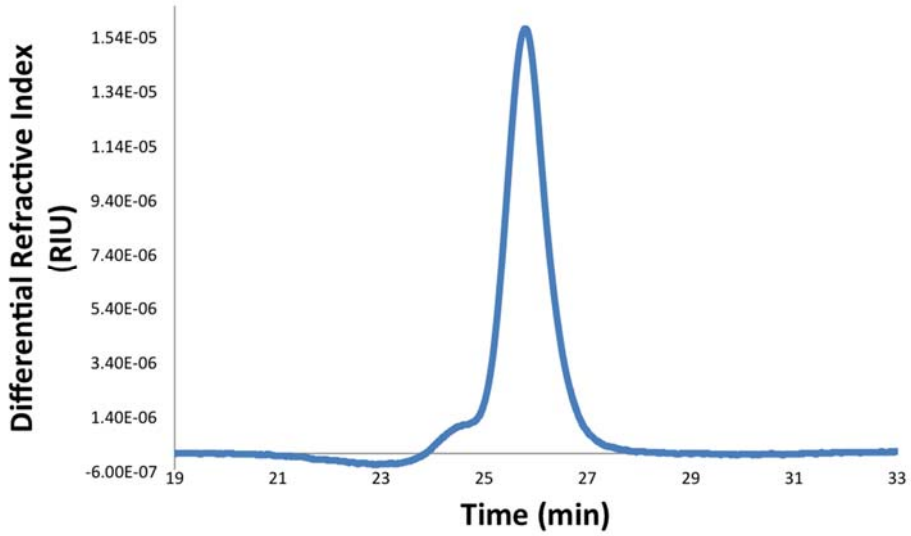

Figure S41. Polymerization of 158 equivalents of ε-caprolactone by compound [(fc^{P,B})Zn(μ-OCH$_2$Ph)]$_2$; M_n = 8,900; $Đ$ = 1.09; related to Table 1, entry 3.

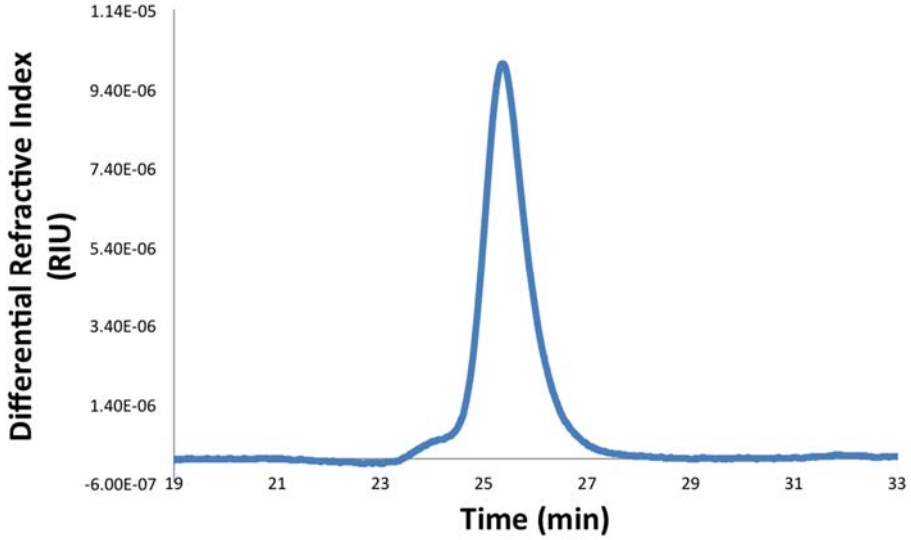

Figure S42. Polymerization of 188 equivalents of ε-caprolactone by compound [(fc^{P,B})Zn(μ-OCH$_2$Ph)]$_2$[BAr^F]$_2$; M_n = 10,500; $Đ$ = 1.08; related to Table 1, entry 4.

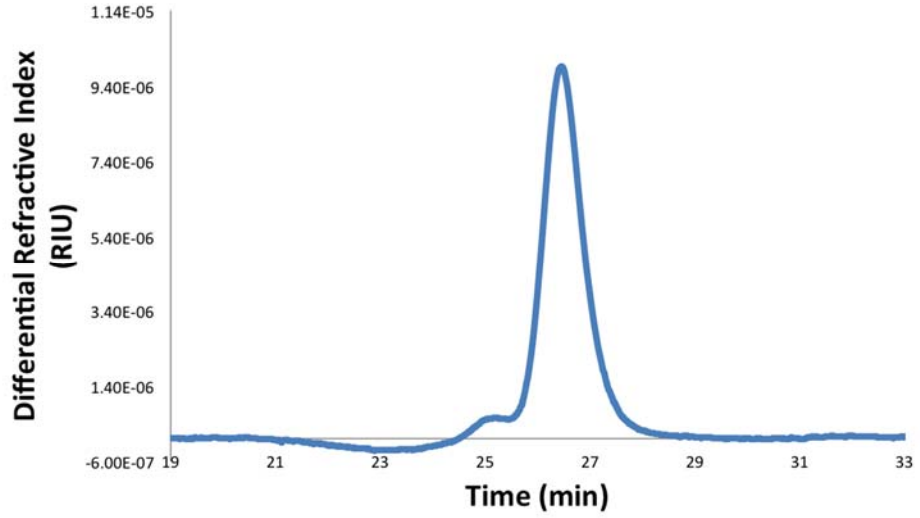

Figure S43. Polymerization of 194 equivalents of trimethylene carbonate by compound $[(fc^{P,B})Zn(\mu\text{-}OCH_2Ph)]_2$; M_n = 10,000; $Đ$ = 1.14; related to Table 1, entry 5.

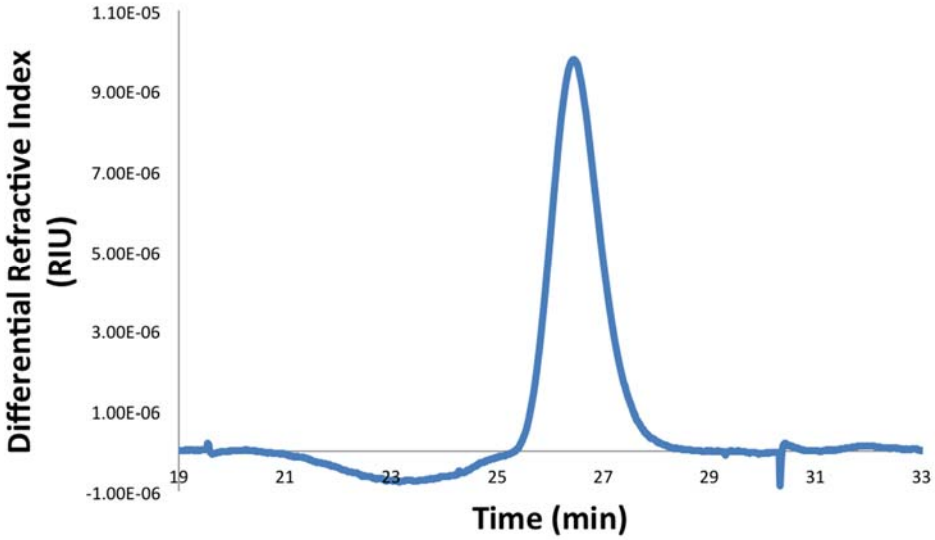

Figure S44. Polymerization of 156 equivalents of trimethylene carbonate by compound $[(fc^{P,B})Zn(\mu\text{-}OCH_2Ph)]_2[BAr^F]_2$; M_n = 8,100; $Đ$ = 1.02; related to Table 1, entry 6.

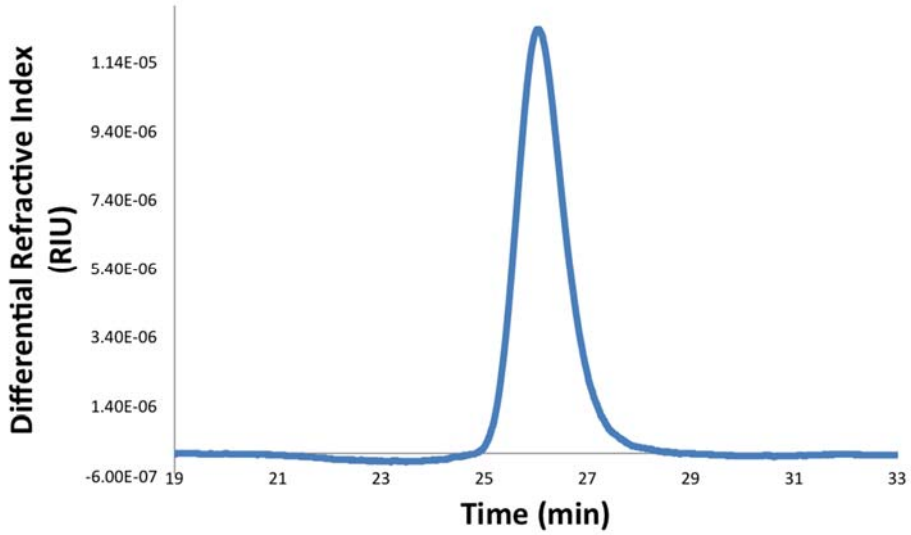

Figure S45. Polymerization of 204 equivalents of δ-valerolactone by compound [(fc^{P,B})Zn(μ-OCH$_2$Ph)]$_2$; M_n = 10,400; $Đ$ = 1.01; related to Table 1, entry 7.

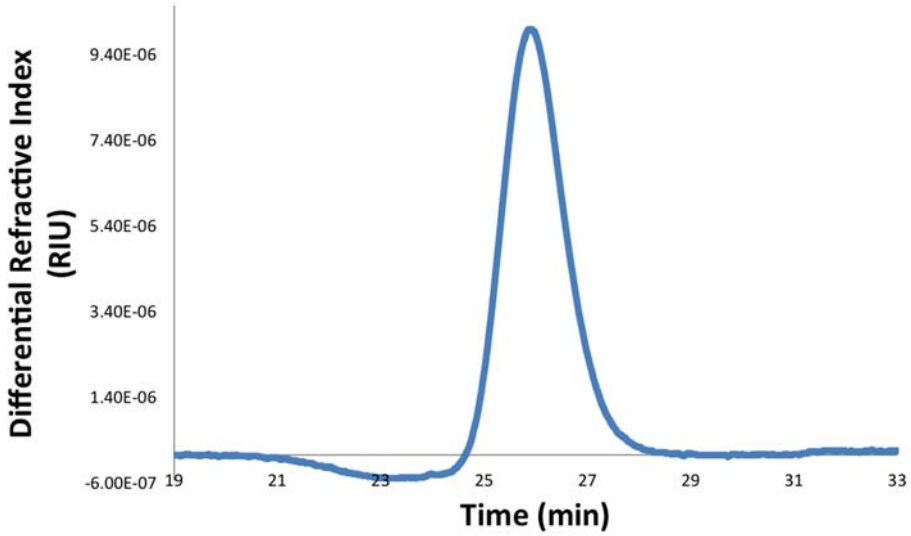

Figure S46. Polymerization of 202 equivalents of δ-valerolactone by compound [(fc^{P,B})Zn(μ-OCH$_2$Ph)]$_2$[BAr^F]$_2$; M_n = 10,500; $Đ$ = 1.04; related to Table 1, entry 8.

Conversion Studies

Table S1. Molar mass versus conversion study of L-lactide in the presence of $[(fc^{P,B})Zn(OCH_2Ph)]_2[BAr^F]_2$; related to Table 1.

Time (min)	Conversion (%)	M_n (NMR)	M_n (SEC)	*Đ*
35	25	10,500	11,800	1.05
55	36	14,300	15,500	1.08
75	43	17,100	18,600	1.06
95	49	19,700	20,900	1.11
115	55	22,600	22,800	1.05

Conditions: benzene as a solvent (1.5 mL) and hexamethylbenzene as an internal standard. The experiment was performed at 70 °C.

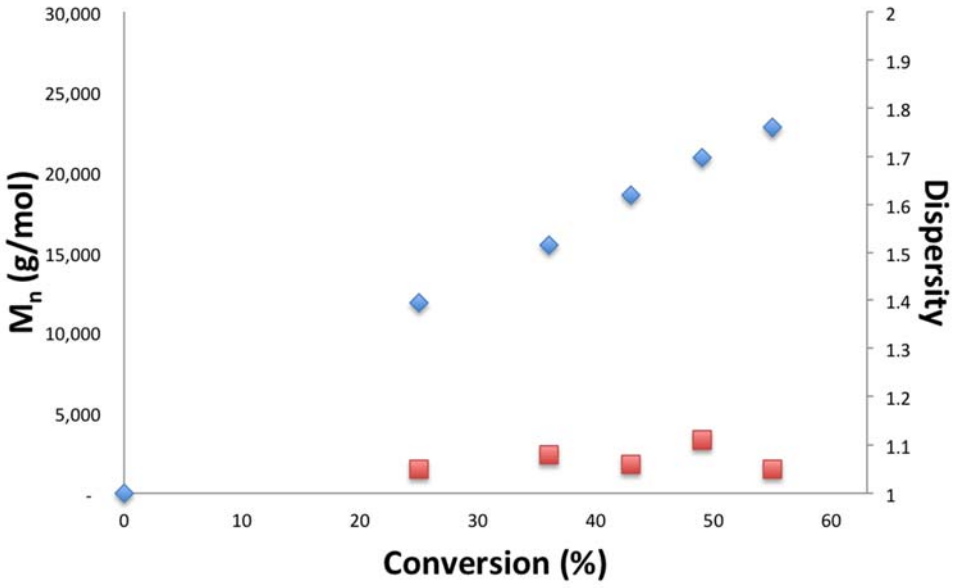

Figure S47. Conversion of L-lactide versus M_n in the presence of $[(fc^{P,B})Zn(OCH_2Ph)]_2[BAr^F]_2$; related to Table 1.

Table S2. Molar mass versus conversion study of trimethylene carbonate in the presence of $[(fc^{P,B})Zn(OCH_2Ph)]_2[BAr^F]_2$; related to Table 1.

Time (min)	Conversion (%)	M_n (NMR)	M_n (SEC)	*Đ*
2	20	3,500	3,100	1.09
3	35	5,900	5,800	1.01
4	41	7,000	7,100	1.02
5	43	7,300	7,600	1.04
6	48	8,200	8,800	1.00
7	68	12,100	12,200	1.02

Conditions: benzene as a solvent (1.5 mL) and hexamethylbenzene as an internal standard. The experiment was performed at ambient temperature.

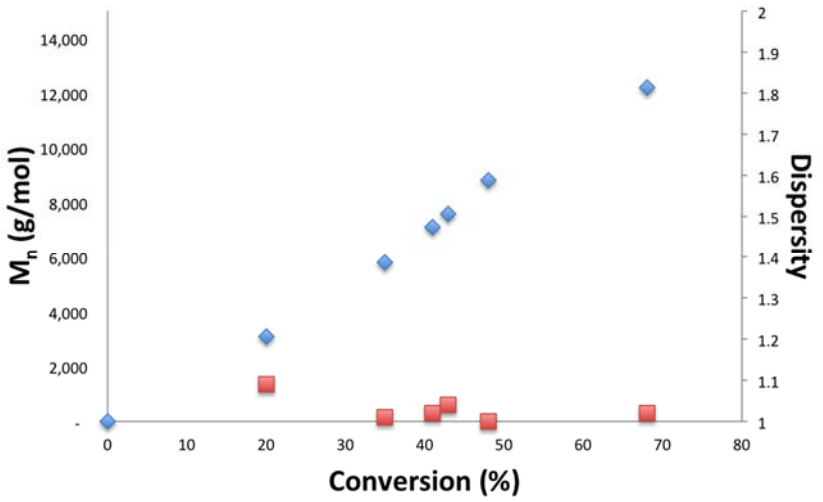

Figure S48. Conversion of trimethylene carbonate versus M_n in the presence of $[(fc^{P,B})Zn(OCH_2Ph)]_2[BAr^F]_2$; related to Table 1.

Table S3. Molar mass versus conversion study of δ-valerolactone in the presence of $[(fc^{P,B})Zn(OCH_2Ph)]_2$; related to Table 1.

Time (min)	Conversion (%)	M_n (NMR)	M_n (SEC)	*Đ*
10	21	6,000	5,800	1.03
15	30	8,000	7,400	1.01
25	48	13,000	11,800	1.04
30	58	15,800	14,100	1.03
35	65	17,900	15,900	1.04
40	71	18,800	16,900	1.04

Conditions: benzene as a solvent (1.5 mL) and hexamethylbenzene as an internal standard. The experiment was performed at ambient temperature.

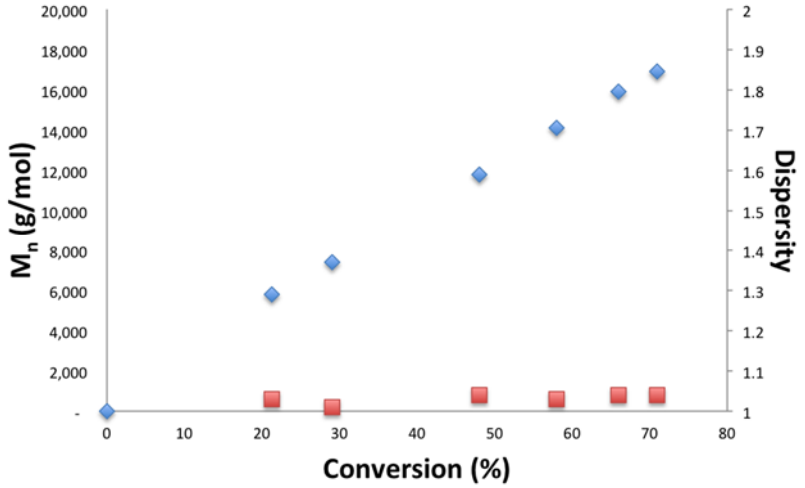

Figure S49. Conversion of δ-valerolactone versus M_n in the presence of $[(fc^{P,B})Zn(OCH_2Ph)]_2$; related to Table 1.

Table S4. Molar mass versus conversion study of δ-valerolactone in the presence of [(fc^{P,B})Zn(OCH$_2$Ph)]$_2$[BAr^F]$_2$; related to Table 1.

Time (min)	Conversion (%)	M_n (NMR)	M_n (SEC)	*Đ*
2	27	8,300	8,900	1.1
4	36	10,900	11,900	1.04
6	40	12,100	13,200	1.04
8	44	13,500	14,700	1.04
10	49	15,000	16,300	1.02
12	56	16,700	17,700	1.03
14	61	17,800	18,500	1.02

Conditions: benzene as a solvent (1.5 mL) and hexamethylbenzene as an internal standard. The experiment was performed at ambient temperature.

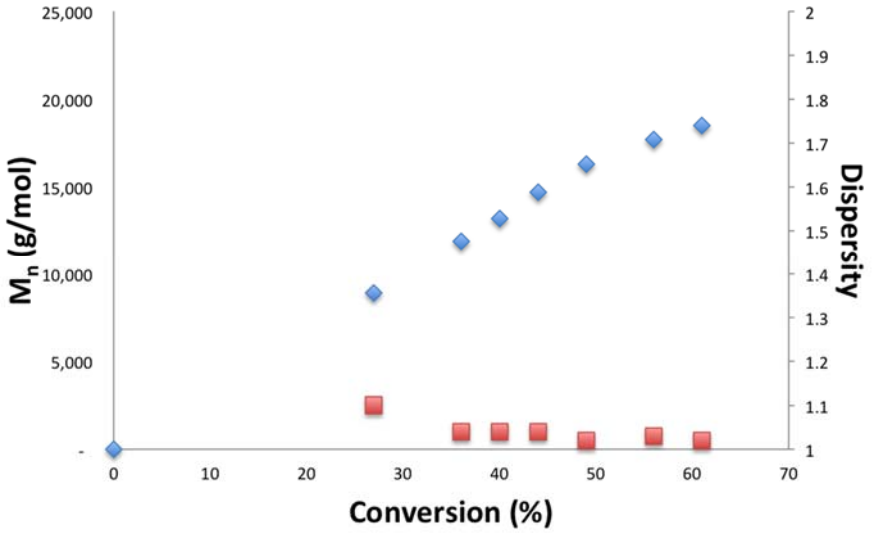

Figure S50. Conversion of δ-valerolactone versus M_n in the presence of [(fc^{P,B})Zn(OCH$_2$Ph)]$_2$[BAr^F]$_2$; related to Table 1.

Table S5. Molar mass versus conversion study of ε-caprolactone in the presence of [(fc^{P,B})Zn(OCH$_2$Ph)]$_2$; related to Table 1.

Time (min)	Conversion (%)	M_n (NMR)	M_n (SEC)	*Đ*
60	15	5,100	5,100	1.01
120	25	8,900	8,300	1.02
180	32	11,300	10,100	1.01
240	43	15,100	14,000	1.01
300	52	18,100	16,400	1.01
360	57	19,800	18,100	1.01

Conditions: benzene as a solvent (1.5 mL) and hexamethylbenzene as an internal standard. The experiment was performed at ambient temperature.

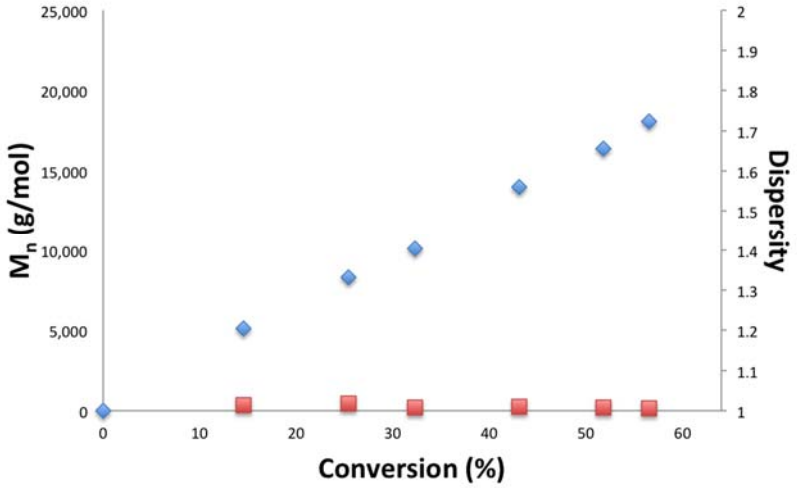

Figure S51. Conversion of ε-caprolactone versus M_n in the presence of $[(fc^{P,B})Zn(OCH_2Ph)]_2$; related to Table 1.

Table S6. Molar mass versus conversion study of ε-caprolactone in the presence of $[(fc^{P,B})Zn(OCH_2Ph)]_2[BAr^F]_2$; related to Table 1.

Time (min)	Conversion (%)	M_n (NMR)	M_n (SEC)	*Đ*
60	17	6,000	5,700	1.06
120	30	10,500	9,300	1.09
180	46	16,100	16,200	1.03
240	57	19,900	20,000	1.04
300	68	23,800	23,800	1.02
360	75	26,200	26,300	1.02

Conditions: benzene as a solvent (1.5 mL) and hexamethylbenzene as an internal standard. The experiment was performed at ambient temperature.

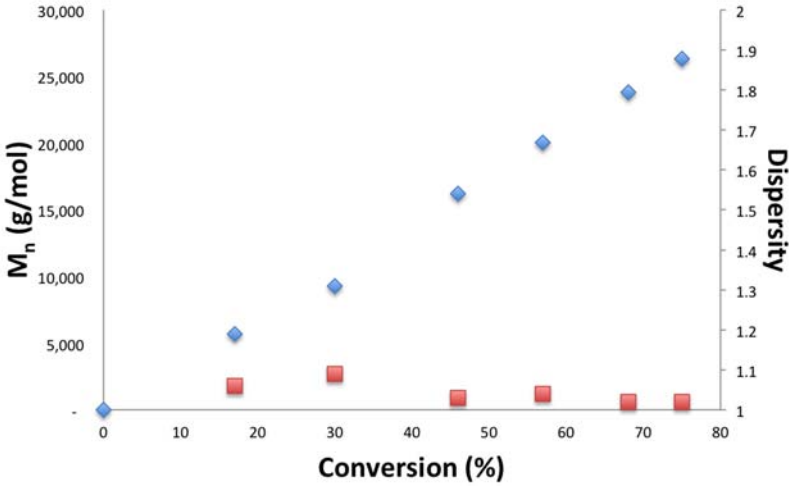

Figure S52. Conversion of ε-caprolactone versus M_n in the presence of $[(fc^{P,B})Zn(OCH_2Ph)]_2[BAr^F]_2$; related to Table 1.

DFT Calculations (Frisch, 2010)

Table S7. **Energies, enthalpies, and free energies of the structures calculated at the PBE1PBE/SDD, 6-311+G(d,p) (PCM, GD3, benzene)//B3LYP/LANL2DZ, 6-31G(d) level;** related to Figures 5-7.

Structures	ΔH	ΔG	G	E with corrections	new G with corrections
Cat-monomer-1	0.43718	0.345	-1587.434324	-1748.702933	-1748.357933
Cat-monomer-2	0.437257	0.344178	-1587.424939	-1748.716437	-1748.372259
After-insertion-LA-dimer	1.031576	0.837546	-3709.203046	-4031.463474	-4030.625928
After-insertion-LA-monomer	0.591316	0.470926	-2121.704113	-2282.701359	-2282.230433
I	0.875768	0.706086	-3174.908168	-3497.482632	-3496.776546
TSI-II	0.989208	0.807349	-3556.520989	-3878.906822	-3878.099473
II	0.99036	0.805784	-3556.557152	-3878.90713	-3878.101346
TSII-III	0.989663	0.808934	-3556.548578	-3878.897142	-3878.088208
III	0.990874	0.803592	-3556.564162	-3878.909919	-3878.106327
IV	0.991638	0.802899	-3556.575983	-3878.920882	-3878.117983
TMC	0.111273	0.074079	-381.634182	-381.4101659	-381.3360869
Lactide	0.151554	0.105907	-534.250539	-533.935059	-533.829152

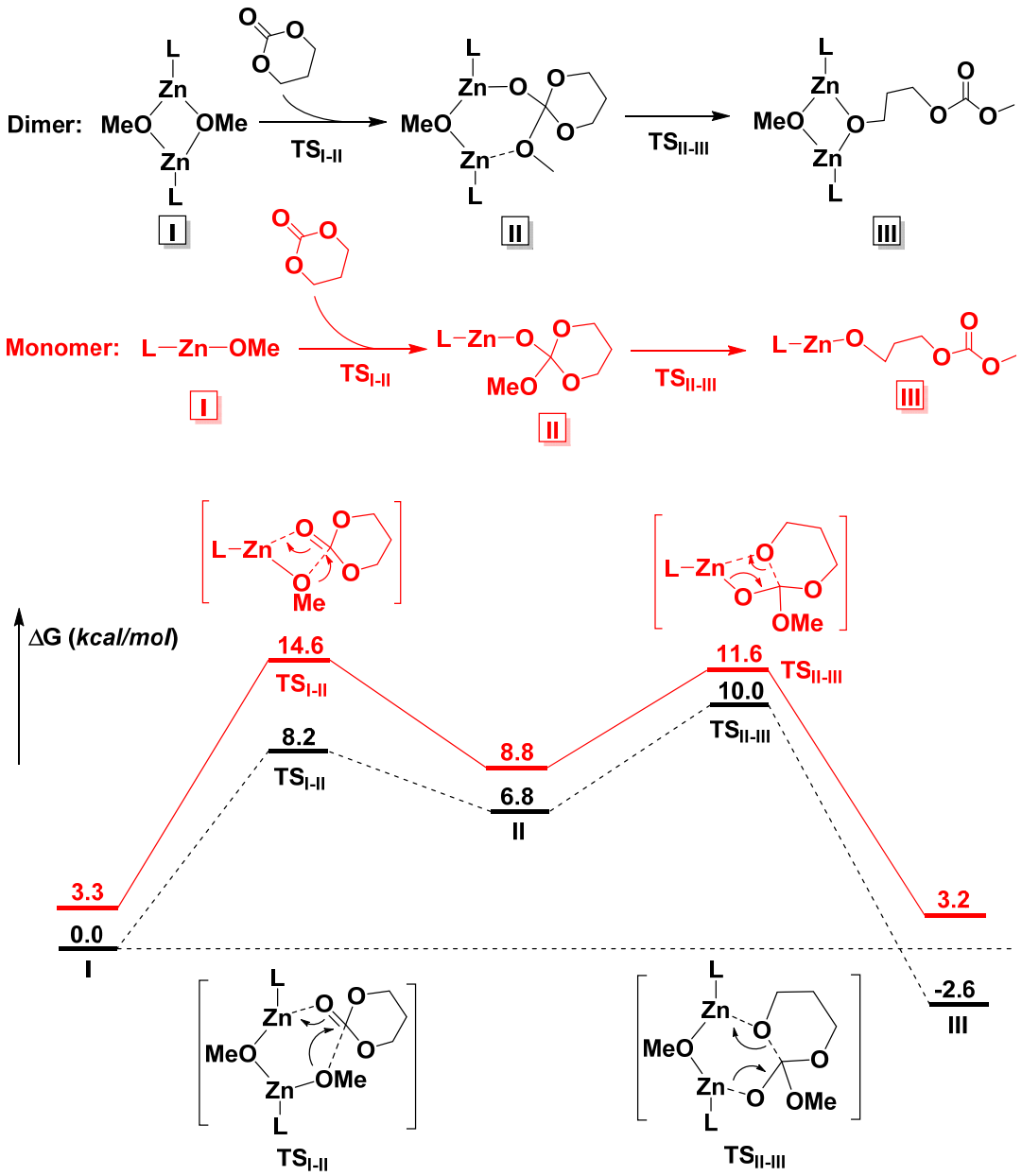

Figure S53. Comparison of the initiation steps of TMC polymerization catalyzed by a monomeric (red) or dimeric (black) form of the zinc complex; figure adapted from (Abubekerov et al., 2018); related to Figure 7.

References

ABUBEKEROV, M. & DIACONESCU, P. L. 2015. Synthesis and Characterization of Ferrocene-Chelating Heteroscorpionate Complexes of Nickel(II) and Zinc(II). *Inorg. Chem.,* 54**,** 1778–1784.

ABUBEKEROV, M., WEI, J., SWARTZ, K. R., XIE, Z., PEI, Q. & DIACONESCU, P. L. 2018. Preparation of multiblock copolymers via step-wise addition of l-lactide and trimethylene carbonate. *Chem. Sci.,* 9**,** 2168-2178.

BECKE, A. D. 1993a. Density-functional thermochemistry. III. The role of exact exchange. *J. Chem. Phys.,* 98**,** 5648-5652.

BECKE, A. D. 1993b. A new mixing of Hartree–Fock and local density-functional theories. *J. Chem. Phys.,* 98**,** 1372-1377.

COCOCCIONI, M. & DE GIRONCOLI, S. 2005. Linear response approach to the calculation of the effective interaction parameters in the $\mathrm{LDA}+\mathrm{U}$ method. *Phys. Rev. B,* 71**,** 035105.

DHAR, D., YEE, G. M., SPAETH, A. D., BOYCE, D. W., ZHANG, H., DERELI, B., CRAMER, C. J. & TOLMAN, W. B. 2016. Perturbing the Copper(III)–Hydroxide Unit through Ligand Structural Variation. *J. Am. Chem. Soc.,* 138**,** 356-368.

DITCHFIELD, R., HEHRE, W. J. & POPLE, J. A. 1971. Self-Consistent Molecular-Orbital Methods. IX. An Extended Gaussian-Type Basis for Molecular-Orbital Studies of Organic Molecules. *J. Chem. Phys.,* 54**,** 724-728.

DOLG, M., WEDIG, U., STOLL, H. & PREUSS, H. 1987. Energy-adjusted abinitio pseudopotentials for the first row transition elements. *J. Chem. Phys.,* 86**,** 866-872.

EHLERS, A. W., BÖHME, M., DAPPRICH, S., GOBBI, A., HÖLLWARTH, A., JONAS, V., KÖHLER, K. F., STEGMANN, R., VELDKAMP, A. & FRENKING, G. 1993. A set of f-polarization functions for pseudo-potential basis sets of the transition metals Sc · Cu, Y · Ag and La · Au. *Chem. Phys. Lett.,* 208**,** 111-114.

FRISCH, M. J. T., G. W.; SCHLEGEL, H. B.; SCUSERIA, G. E.; ROBB, M. A.; CHEESEMAN, J. R.; SCALMANI, G.; BARONE, V.; MENNUCCI, B.; PETERSSON, G. A.; NAKATSUJI, H.; CARICATO, M.; LI, X.; HRATCHIAN, H.P.; IZMAYLOV, A. F.; BLOINO, J.; ZHENG, G.; SONNENBERG, J. L.; HADA, M.; EHARA, M.; TOYOTA, K.; FUKUDA, R.; HASEGAWA, J.; ISHIDA, M.; NAKAJIMA, T.; HONDA, Y.; KITAO, O.; NAKAI, H.; VREVEN, T.; MONTGOMERY, JR., J. A.; PERALTA, J. E.; OGLIARO, F.; BEARPARK, M.; HEYD, J. J.; BROTHERS, E.; KUDIN, K. N.; STAROVEROV, V. N.; KOBAYASHI, R.; NORMAND, J.; RAGHAVACHARI, K.; RENDELL, A.; BURANT, J. C.; IYENGAR, S. S.; TOMASI, J.; COSSI, M.; REGA, N.; MILLAM, N. J.; KLENE, M.; KNOX, J. E.; CROSS, J. B.; BAKKEN, V.; ADAMO, C.; JARAMILLO, J.; GOMPERTS, R.; STRATMANN, R. E.; YAZYEV, O.; AUSTIN, A. J.; CAMMI, R.; POMELLI, C.; OCHTERSKI, J. W.; MARTIN, R. L.; MOROKUMA, K.; ZAKRZEWSKI, V. G.; VOTH, G. A.; SALVADOR, P.; DANNENBERG, J. J.; DAPPRICH, S.; DANIELS, A. D.; FARKAS, Ö.; FORESMAN, J. B.; ORTIZ, J. V.; CIOSLOWSKI, J.; FOX, D. J. 2010. Gaussian 09. Wallingford, CT: Gaussian Inc.

GRIMME, S., ANTONY, J., EHRLICH, S. & KRIEG, H. 2010. A consistent and accurate ab initio parametrization of density functional dispersion correction (DFT-D) for the 94 elements H-Pu. *J. Chem. Phys.,* 132**,** 154104.

HARIHARAN, P. C. & POPLE, J. A. 1973. The influence of polarization functions on molecular orbital hydrogenation energies. *Theor. Chim. Acta,* 28**,** 213-222.

HAY, P. J. & WADT, W. R. 1985. Ab initio effective core potentials for molecular calculations. Potentials for K to Au including the outermost core orbitals. *J. Chem. Phys.,* 82**,** 299-310.

HEHRE, W. J., DITCHFIELD, R. & POPLE, J. A. 1972. Self-Consistent Molecular Orbital Methods. XII. Further Extensions of Gaussian—Type Basis Sets for Use in Molecular Orbital Studies of Organic Molecules. *J. Chem. Phys.,* 56**,** 2257-2261.

LEE, C., YANG, W. & PARR, R. G. 1988. Development of the Colle-Salvetti correlation-energy formula into a functional of the electron density. *Phys. Rev. B,* 37**,** 785.

MATSUO, J., AOKI, K., SANDA, F. & ENDO, T. 1998. Substituent Effect on the Anionic Equilibrium Polymerization of Six-Membered Cyclic Carbonates. *Macromolecules,* 31**,** 4432-4438.

PANGBORN, A. B., GIARDELLO, M. A., GRUBBS, R. H., ROSEN, R. K. & TIMMERS, F. J. 1996. Safe and Convenient Procedure for Solvent Purification. *Organometallics,* 15**,** 1518-1520.

PAOLO, G., STEFANO, B., NICOLA, B., MATTEO, C., ROBERTO, C., CARLO, C., DAVIDE, C., GUIDO, L. C., MATTEO, C., ISMAILA, D., ANDREA DAL, C., STEFANO DE, G., STEFANO, F., GUIDO, F., RALPH, G., UWE, G., CHRISTOS, G., ANTON, K., MICHELE, L., LAYLA, M.-S., NICOLA, M., FRANCESCO, M., RICCARDO, M., STEFANO, P., ALFREDO, P., LORENZO, P., CARLO, S., SANDRO, S., GABRIELE, S., ARI, P. S., ALEXANDER, S., PAOLO, U. & RENATA, M. W. 2009. QUANTUM ESPRESSO: a modular and open-source software project for quantum simulations of materials. *J. Phys. Condens. Matter,* 21**,** 395502.

PERDEW, J. P., BURKE, K. & ERNZERHOF, M. 1996. Generalized Gradient Approximation Made Simple. *Phys. Rev. Lett.,* 77**,** 3865-3868.

ROY, L. E., HAY, P. J. & MARTIN, R. L. 2008. Revised Basis Sets for the LANL Effective Core Potentials. *J. Chem. Theory Comput.,* 4**,** 1029-1031.

SCALMANI, G. & FRISCH, M. J. 2010. Continuous surface charge polarizable continuum models of solvation. I. General formalism. *J. Chem. Phys.,* 132**,** 114110.